A STUDY OF PVD BI-LAYER CUTTING TOOL COATINGS USED FOR MACHINING OF SUPER DUPLEX STAINLESS STEEL

A STUDY OF PVD BI-LAYER CUTTING TOOL COATINGS USED FOR MACHINING OF SUPER DUPLEX STAINLESS STEEL

By

LUCAS MONTEIRO LIMA, B. Eng

A Thesis Submitted to the School of Graduate Studies in Partial Fulfilment of the Requirements
for the Degree Master of Applied Science

McMaster University, Hamilton, Ontario, Canada

MASTER OF APPLIED SCIENCE (2020)
(MECHANICAL ENGINEERING)

McMaster University
Hamilton, Ontario, Canada

TITLE: A STUDY OF PVD BI-LAYER CUTTING TOOL COATINGS USED FOR MACHINING OF SUPER DUPLEX STAINLESS STEEL

AUTHOR: Lucas Monteiro Lima, B. Eng., Mechanical Engineering

SUPERVISOR: Dr. Stephen C. Veldhuis

Department of Mechanical Engineering

McMaster University

NUMBER OF PAGES: xiii, 95

ABSTRACT

The oil and gas industry places intensive demands on materials due to the corrosive environments they work in and the heavy loads and wear conditions they apply. Materials such as Super Duplex Stainless Steel (SDSS) are widely used for this purpose, since their chemical composition, corrosion resistance and mechanical properties enable them to sustain the severe conditions associated with petroleum extraction. However, machining this material presents a significant challenge due to the high temperatures and stresses generated during the cutting process, which result in rapid tool wear. To address this challenge, a series of Physical Vapour Deposition (PVD) bi-layer multifunctional coatings were developed to improve tool performance during SDSS machining. Bi-layer coatings consist of two layers, each of which is designed to address various wear phenomena observed during machining. In addition, the cutting performance of the latest generation of PVD coating deposition methods known as High-Power Impulse Magnetron Sputtering (HiPIMS) was evaluated. This study investigated the effect of different HiPIMS bi-layer coatings on the wear performance of cutting tools during finish turning of SDSS.

ACKNOWLEDGEMENT

I would first like to express my deepest gratitude to my supervisor Dr. Stephen Veldhuis, not only for his expertise and support but also for the many learning opportunities offered me through different projects.

Secondly, I wish to express my sincere appreciation to: Dr. German Fox-Rabinovich, who has the substance of a genius and has convincingly guided me through this work; Dr Jose Mario Paiva for his guidance and friendship over many years; Dr. Julia Dosbaeva for her aid in many characterizations and counseling; Dr. Arif Abul for his guidance and feedback; the MMRI staff for supporting with analysis and training of many processes.

I also would like to thank all friends and colleagues that I made in Canada which provided me with stimulating discussions as well as happy distractions to rest my mind outside of my research.

In addition, I would like to thank my family and friends back home, for their wise counsel, sympathetic ear, support, and endless love in these difficult times. My special thanks should also go to my grandfather. His memory will forever be with me.

Last but not least, I gratefully acknowledge that this research was supported by the Natural Sciences and Engineering Research Council of Canada (NSERC) under the CANRIMT Strategic Research Network Grant.

CONTENTS

LIST OF FIGURES

LIST OF TABLES

NOMENCLATURE

SDSS – Super Duplex Stainless Steel

PREn – Pitting Resistance Equivalent Number

PSDZ – Primary Shear Deformation Zone

SSDZ – Secondary Shear Deformation Zone

TSDZ – Tertiary Shear Deformation Zone

BUE – Built up Edge

AlTiN – Aluminum Titanium Nitride

TiB_2 – Titanium Diboride

WC/C – Tungsten Carbide Carbon

CrN – Chromium Nitride

THESIS OUTLINE

This research work consists of the following six chapters:

I. **Introduction:** This chapter outlines the motivation and research objectives of this thesis.

II. **Literature Review:** A description of the structural characteristics of SDSS, the basics of the metal cutting process and other information related to the subject.

III. **Experimental Procedure:** The methodology, experimental setups as well as parameters of the sample tests are outlined in this chapter, which is subdivided into 4 topics: Workpiece characterization, coating characterization, machining performance and chip analysis.

IV. **Results and Discussion:** The results obtained from the experimental studies as well as discussion of the observed behaviors and phenomena are presented in this chapter.

V. **Conclusions:** The main conclusions of this research are drawn from the previously disclosed experimental results and discussion.

VI. **Suggestion to future works:** This chapter provides suggestions for further research directions in this field.

CHAPTER 1 – INTRODUCTION:

Oil and gas commodities account for a considerable portion of the global gross domestic product (GDP) and are one of the primary sources of energy. Considered to be the largest sector in the world in terms of dollar value, the oil and gas industry play a critical role in multiple supply chains. Since offshore oil reserves can range as far as 300km from the coast and reach depths of up to 7 km, under a thick layer of salt, marine water and minerals, the necessity for specific materials becomes apparent. Such materials need to be capable of maintaining their structural properties under extremely hazardous subsurface maritime conditions, where sea currents as well as external and internal pressures produce a corrosive environment and high mechanical loads.

These operating environment factors make super duplex stainless steel a preferable material for usage in the oil and gas sector, due to their high concentration of Chromium, Molybdenum as well as Nitrogen content. These properties provide the material component with an elevated pitting corrosion resistance and mechanical strength. In machining operations however, these steel grades feature a high tendency of work hardening and poor thermal conductivity, due to their amplification of the heat generated at the cutting zone, which can alter the microstructure of the material. The cutting process is characterized by high adhesion of the workpiece to the cutting tool, high cutting temperatures as well as issues concerning chip formation, all of which ultimately result in a very short tool life.

1.1 Motivation

Over the years, the use of super duplex stainless steel has increased due to the growing demand for petroleum extraction. The energy sector requires materials which are capable of resisting corrosion in the severe subsurface naval environment.

Figure 1 and 2 provide an overview of how the demand for petroleum extraction has increased over the years. As a consequence of this, the demand for materials which are able to sustain the quite aggressive operative environments has grown. One example of such materials is the family of duplex & super duplex stainless steels.

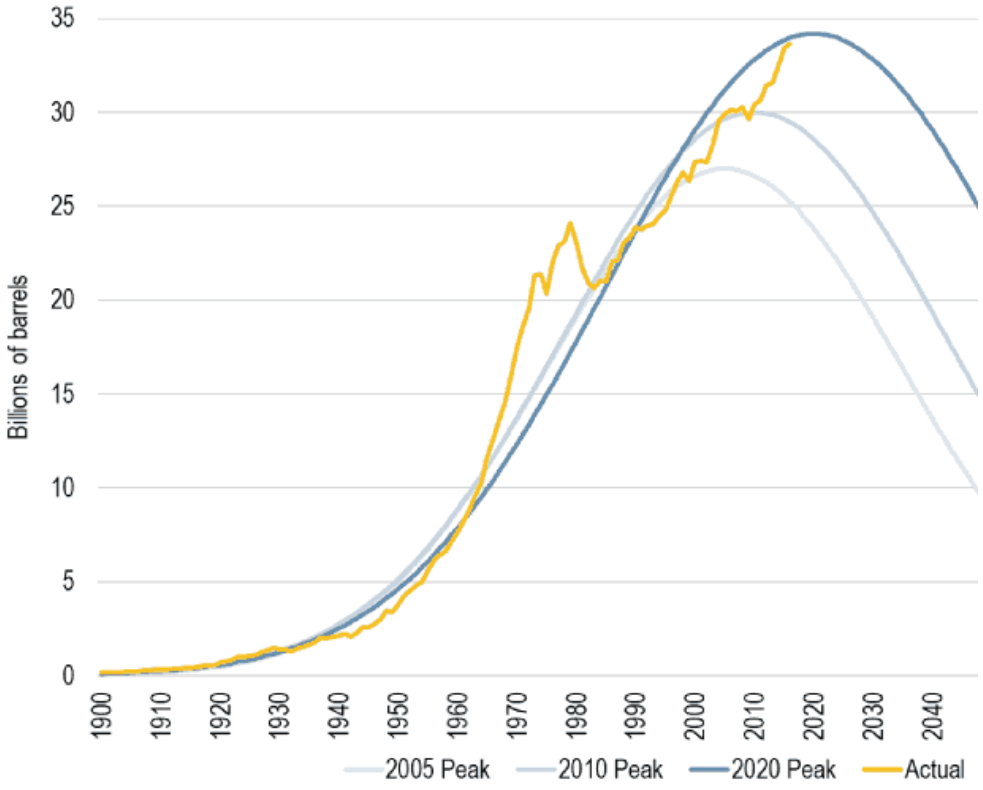

Figure 1. World Annual Oil Production (1900-2016) and Peak Oil (2005-2020 Scenarios) [adapted from 1]

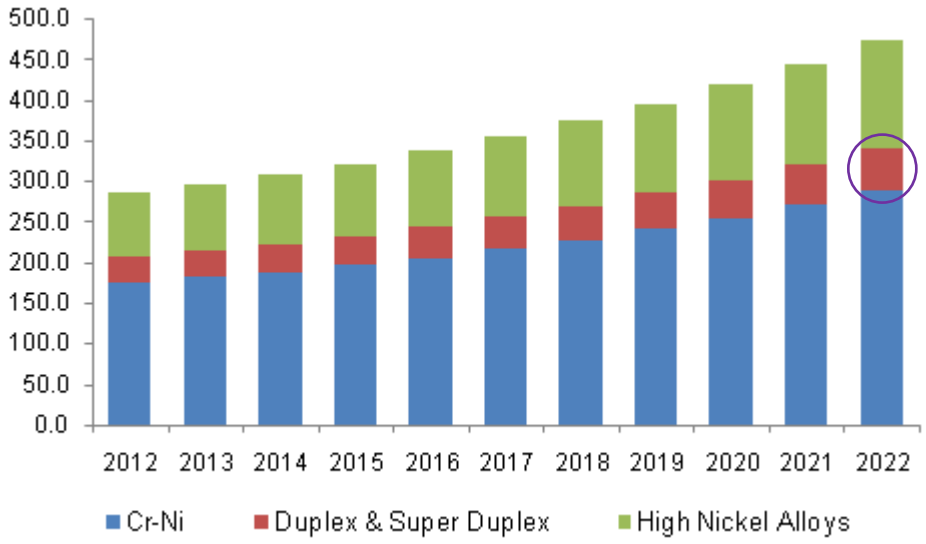

Figure 2. U.S. stainless steel round Bar market volume, by product, 2012-2022, (Kilo Tons) [2]

However, since super duplex stainless steels contain a two-phase ferrite and austenite structure, they tend to have a high work hardening rate [3]. These properties make the machinability of super duplex stainless steel challenging due to the considerable number of issues such as frequent vibration chatter, gumming of tools and poor chip breaking [3,4]. A combination of these issues drastically decreases the tool's operating life and impose significant additional machining costs.

Wear performance needs to be discussed in detail since it offers considerable potential for future studies. Therefore, this study will outline the specifics of this material's machining as well as propose some solutions to its aforementioned problems.

1.2 Research Objectives

The aim of this study is to investigate the impact of different HiPIMS bi-layer coatings on the wear performance of the cutting tools during the turning of super duplex stainless steel. The research objectives of this work are the following:

1. Investigation of the tool life and wear mechanisms of bi-layer lubricious PVD applied AlTiN + TiB_2 and AlTiN + WC/C coatings and the uncoated tool in comparison with a commercially available benchmark monolayer PVD coating (AlTiN – Balzers).

2. Investigation of the tool life and wear mechanisms of bi-layer PVD applied AlTiN + TiB_2 and AlTiN + CrN coatings compared to a commercially available benchmark monolayer PVD coating (AlTiN – Balzers) under high cutting speeds.

3. Evaluation of the chips obtained from the use of the different coatings. This will be achieved through the comparison of microstructural characteristics, micro-hardness, chip thickness measurements, undersurface morphology and shear band analysis throughout the cross section of each coated tool.

4. Evaluation of the mechanical properties of the proposed coatings in terms of surface morphology, micro-hardness, adhesion, elastic modulus, residual stresses as well as coating thickness and architecture. This will be carried out by SEM cross section analysis for each coated tool.

CHAPTER 2 – LITERATURE REVIEW

2.1 SUPER DUPLEX STAINLESS STEELS

2.1.1 – General Characteristics

Super duplex Stainless Steels (SDSS) are a type of stainless steel engineered for applications such as oil & gas components, which operate under an aggressively corrosive environment characterized by the high presence of chlorides in seawater that could cause pitting. High mechanical loads should also be kept in mind while engineering this material, since it is expected to function under depths of up to 7km below the surface. [5]

An empirical approach of quantifying pitting corrosion resistance and classifying duplex stainless and super duplex stainless steel is through the Pitting Resistance Equivalent Number (PREn). This is an equation where the pitting corrosion resistance of different stainless-steel grades can be generally compared, with their compositions given in % of element weight. [6]

$$PREN = \%Cr + 3.3\%Mo + 16\%N \qquad \textbf{Equation 1}$$

Duplex stainless steel has a microstructure that consists of 50% ferrite and 50% austenite, in approximately equal volume fractions [7]. To be considered as duplex stainless steel, the material needs to have a value of PREn greater than 20, whereas super duplex stainless steel needs to reach a value greater than 42, according to the ASTM A890/890M international standard. Super Duplex Stainless steel contains a similar chemical composition compared to duplex stainless steel. However, SDSS has an increased number of elements such as Chromium, Nickel, Molybdenum and Nitrogen, which are mainly responsible for improving resistance to pitting corrosion. This grade exhibits a well-balanced microstructure comprised of ferrite and austenite phases, as can be seen in figure 3.

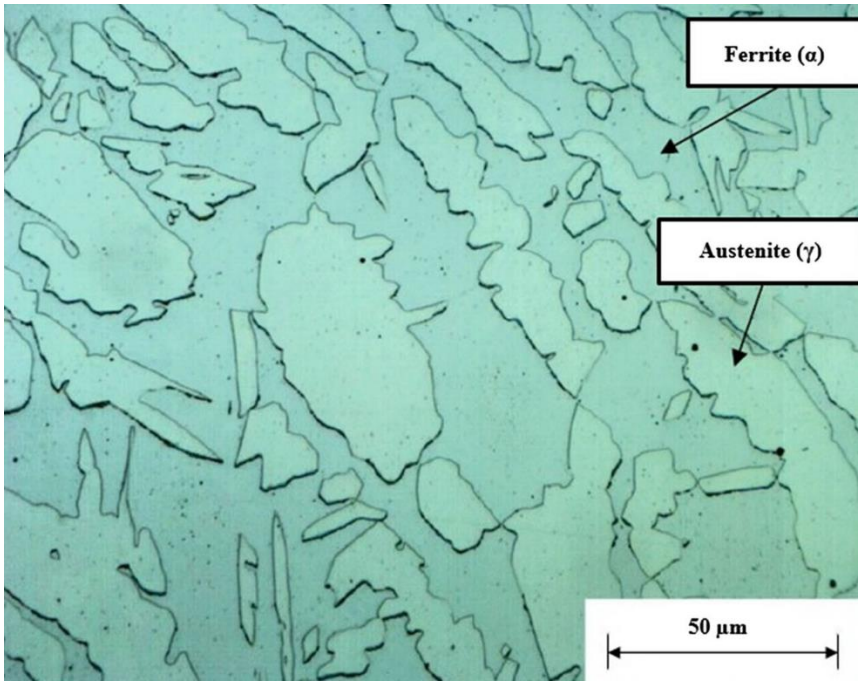

Figure 3. Microstructure of Super Duplex Stainless Steel [used with permission 8]

Use of metal materials makes up 60% of the operational costs of Oil & Gas production and remains important at every step of the industrial chain. The most common type of metal used in the Oil & Gas sector is stainless steel with the inclusion of certain elements such as Nickel and Molybdenum for enhancing corrosion-resistance properties. Table 1 presents the chemical composition of Super Duplex Stainless Steel.

Table 1. Chemical composition of Super Duplex Stainless Steel [7]

Super Duplex Stainless Steel (UNS 32750) Chemical Composition											
Element	Cr	Mo	N	Ni	C	Mn	Si	Cu	P	S	Fe
Weight (%)	25	4	0.3	7	0.03	1.13	0.65	0.78	0.0012	0.018	Balance

Other stainless-steel grades also possess a high resistance to pitting corrosion due to the increased content of as Chromium, Molybdenum and Nitrogen. However, since their microstructural characteristics are not the same, they have other mechanical properties. Figure 4 compares various grades of stainless steel in relation to their Pitting Resistance Equivalent Numbers (PREn).

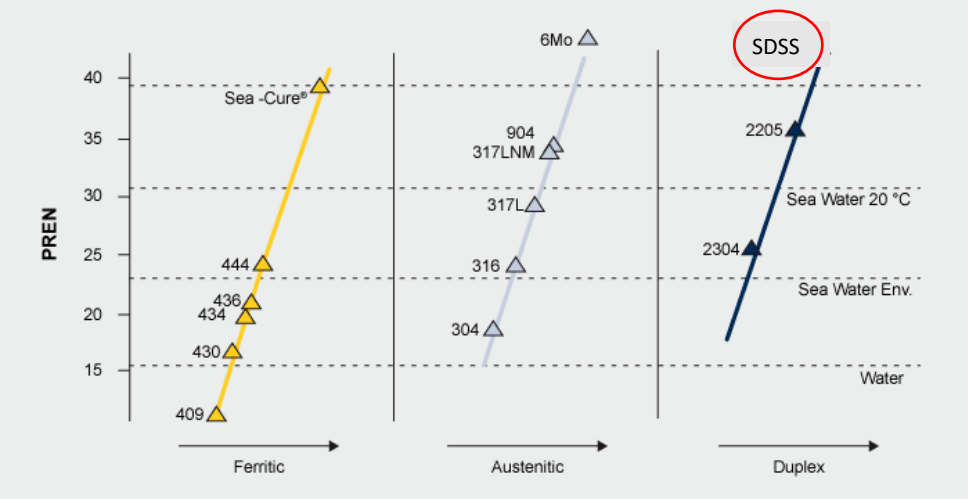

Figure 4. Pitting Resistance Equivalent Number for different stainless-steel grades [adapted from 6]

Although ferritic and austenitic stainless steel offers similar corrosion resistance compared to super duplex stainless steel according to their respective PREn, fine grain microstructure as well as optimal austenite/ferrite content in duplex stainless-steel results in superior mechanical characteristics. This improvement in mechanical properties allows the material to function in high temperature environments. [9]

2.1.2 – Microstructure

The duplex microstructure of SDSS is characterized by the optimal combination of alloying elements and proper heat treatment that results in a dual-phase structure with a roughly equal distribution of ferrite and austenite. The right concentration of alloying elements is necessary to obtain a well-balanced duplex microstructure. [9]

The possible microstructures of SDSS are presented in the Schaeffler diagram (figure 5), which depicts the boundaries of ferrite, austenite and martensite versus varying Chromium and Nickel content. [10]

A Chromium and Nickel equivalent calculation is also possible in the Schaeffler diagram. This equivalent considers other alloying elements that can provide the same effects to the microstructure of stainless steel. [10]

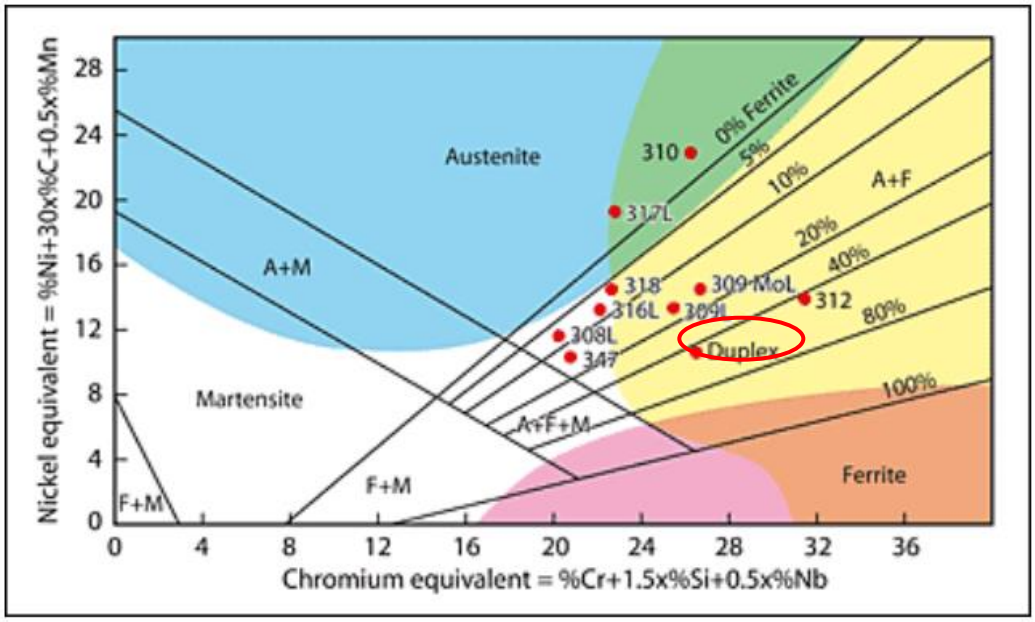

Figure 5. Schaeffler diagram [10]

Scheffler's diagram outlines the microstructures of stainless-steel grades at room temperature. However, when materials are exposed to high temperatures, the thermodynamic equilibrium of their structure is altered, which can lead to the nucleation of undesired secondary phases and precipitates, as well as phase dissolution.

The generation of austenite through the decomposition of ferrite is influenced by the temperature at which it occurs in the solid state. At high temperatures (650-1200ºC) typical for super duplex stainless steel machining, austenite is generated through nucleation and growth. At lower temperatures (300-650º) a non-thermal, martensitic transformation can occur. [11] In light of this, the generated microstructure depends on the chemical composition, cooling, and conditions during heat treatment. The generation of austenite could be partly interrupted if the alloy is being rapidly cooled through the ferritic field [12].

According to the Fe-Cr-Ni system diagram in figure 6, it is possible to visualize the effects of varying temperatures and Cr and Ni components in a Fe system, which lead to the formation of different microstructures, with the boundaries of the duplex microstructure (austenite + ferrite) being highlighted in red.

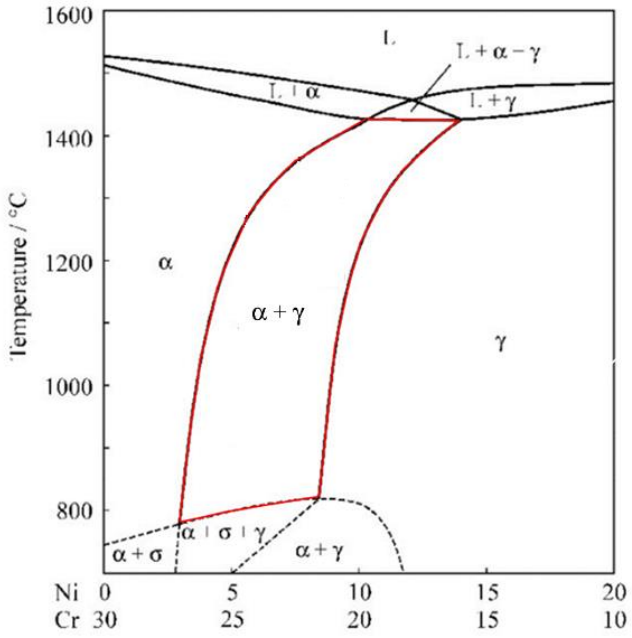

Figure 6. Fe-Cr-Ni diagram [based on 13]

When the material is being operated under different ranges of temperature for a certain period of time, many phases can be generated in the microstructure of super duplex stainless steel that can introduce undesirable qualities in the material. These phases are generated by the thermodynamics of duplex stainless-steel machining. The most common phases are sigma (σ), alpha prime (α') and Chi (χ) phases. Table 2 presents some of these characteristics.

Table 2. Characteristic features of common phases present in super duplex stainless steel [14]

Phase	Precipitation Temperature Range (°C)	Characteristics
Sigma (σ)	600-1000	High Chromium, Molybdenum and Silicon content. Increased hardness and decreased toughness result in a more brittle material.
Alpha prime (α')	350-750	High Chromium content. Formed during the decomposition of ferrite (α -> α'). Increased yield strength and hardness.
Chi (χ)	700-900	High Chromium, Molybdenum, Silicon and Tungsten content. A metastable phase.

Figure 7 shows the formation of several secondary phases in duplex stainless steel, which cause the material to become brittle.

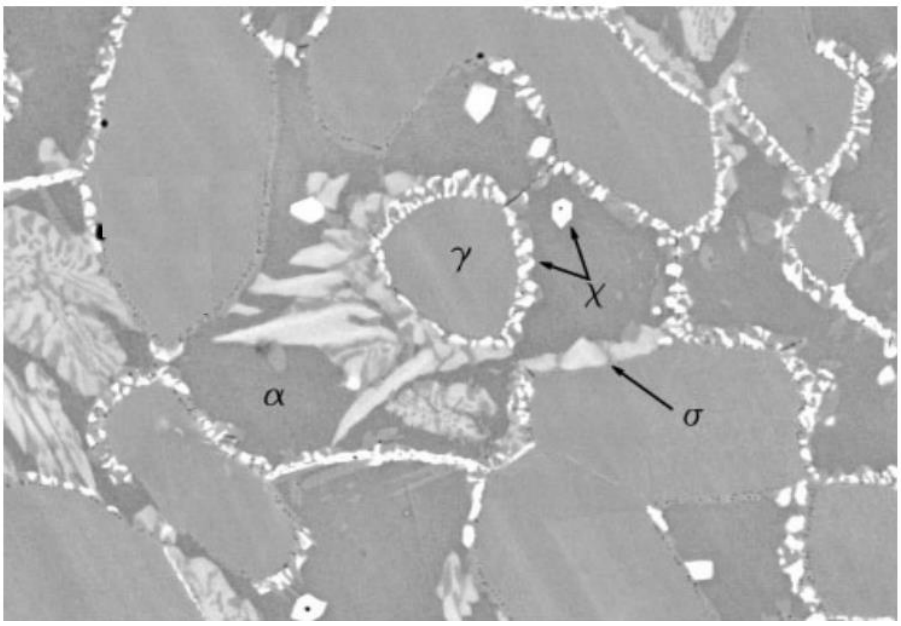

Figure 7. Secondary phases Sigma (σ), alpha (α), Chi (χ) and secondary austenite. [adapted from 15]

2.1.3 – Effects of alloying elements

Chromium is the main alloy component of stainless steel. Stainless steel grades contain at least 11% Chromium [16]. Other elements such as carbon, nickel, molybdenum, copper, titanium, aluminum, silicon, niobium, nitrogen can also be added to obtain certain mechanical characteristics. The addition of these elements will result in the following effects [14], [16]:

- Chromium – The main element responsible for generating a passive layer on the surface of the material which increases its corrosion resistance. The addition of

chromium has a significant impact on the mechanical properties of the alloy, especially hardenability.

- Nickel – Acts as catalyst that accelerates the hardening effect, which enhances the material's ductility. Promotes a stable layer of austenite, leading to the formation of a non-magnetic steel. In addition, nickel also benefits corrosion resistance due to the formation of a Cr-Ni oxide on the surface. It is also frequently used to improve the toughness at low temperatures.
- Molybdenum – In combination with chromium, this element generates a a passive layer on the surface of the material, which improves the pitting corrosion resistance and increases alloy strength at elevated temperatures. By forming durable carbides, molybdenum also increases the hardenability and high temperature sustainability of the alloy.
- Nitrogen – Bolsters the formation of austenitic phases that contribute to a well-balanced microstructure. As a strong austenite promoter, Nitrogen helps improve the corrosion resistance of the austenitic phase.
- Carbon – Enhances hardness and wear resistance through the formation of carbide precipitates. It is usually considered to be the most important alloy element in steel.
- Sulfur – Often considered as an undesirable impurity, it may cause brittleness in the material when present in amounts greater than 0.04%. However, in combination with Mn and in amounts between 0.1% to 0.3%, it forms manganese sulfide (MnS), which tends to actually improve machinability. Such types of materials are often known as free-machining alloys.

- Silicon – Usually present in amounts between 0.5% to 5%, it dissolves in iron and tends to strengthen it. It also improves corrosion resistance and temperature resilience.
- Phosphorus – In general, considered to be an undesirable impurity. Usually it is found in amounts of up to 0.04% in most carbon steels. In hardened steels, it might tend to cause embrittlement.
- Manganese – Increases the hardenability of steel, thereby improving its strength. Usually steels contain at least 0.3% of Mn due to its ability to assist in the deoxidation of the steel, preventing the formation of impurities (inclusions).

2.1.4 – Mechanical Properties

The mechanical properties of super duplex stainless steel are determined by its chemical composition and a structure (combination of the properties of ferrite and austenite). Ferrite has the greatest influence on mechanical characteristics since it has a higher yield strength than austenite. A combination of the enhanced plasticity of austenite and the superior yield strength of ferrite accounts for the mechanical properties of duplex stainless-steel grades. As such, duplex and super duplex stainless steels possess yield strength, at least twice that of austenitic steel. In addition, duplex stainless steels also have a minimum elongation of around 25% [14], [17].

The mechanical behaviour of duplex and super duplex stainless steel is determined by the characteristics of each of their phases. Therefore, the volumetric fractions of austenite and ferrite phases must be brought into equal proportions (50% each) in order to maximize the mechanical properties of the steel. Table 3 shows a comparison of different stainless steels in terms of yield strength, elongation, and hardness.

Table 3. Mechanical properties presented in different stainless steels [18]

Material	AISI / UNS	Yield Strength (MPa)	Ultimate Tensile Strength (MPa)	Elongation (%)
Ferritic	444	275	415	20
Ferritic	430	310	483	22
Duplex	S32304	400	600	25
Super Duplex	**S32750**	**550**	**795**	**25**
Austenitic	304	230	540	45
Austenitic	316	290	580	50

2.1.5 – Physical Properties

The physical properties of super duplex stainless steel are a result of their austenitic and ferritic microstructure. The thermal conductivity of SDSS is usually greater than that of austenitic stainless steel. Duplex stainless steel has lower thermal expansion than austenitic steel due to the presence of a ferritic phase, whereas the other grades exhibit thermal properties closer to those of Carbon Steel [18]. Table 4 compares the thermal conductivity and specific heat of austenitic, ferritic and duplex stainless steels.

Table 4. Physical properties presented in different stainless steels [18]

Material	AISI / UNS	Thermal Conductivity (W/mK)	Specific Heat (kJ/kgK)
Ferritic	444	26.8	0.427
Ferritic	430	23	0.46
Duplex	S32304	17	0.46
Super Duplex	**S32750**	**15**	**0.45**
Austenitic	304	16.2	0.5
Austenitic	316	13	0.49

2.2 Machining

As described by Stephenson et. al [19], industrial metal cutting processes involve the shaping of metal parts through the removal of unwanted material, also known as chips. A wide range of components are produced in this way, from bridges to precise engine parts. Metal cutting consists of many mechanical processes such as grinding, honing, electric discharge, laser machining, and so on. It is one of the most widespread processes of industrial manufacture.

Machining involves a variety of concurrent processes as well as a multitude of variables, which result in different outputs. Therefore, many issues could arise during the course of a machining cycle, such as poor surface integrity, poor tool life and excessive production costs. This section will discuss the major machinability issues related to the machining of hard-to-cut materials such as Super Duplex Stainless Steel and their effect on tool life.

2.2.1 – General Aspects of Metal Cutting

Machining outputs are highly dependent on an instrument's design, tool geometry cutting parameters, phase transformation, heat transfer during cutting, material characteristics, applied coatings and other parameters. Therefore, machining presents a

very complex process that is difficult to predict without taking into consideration all of the aforementioned aspects.

However, all cutting processes function on the same mechanical basis. Figure 8 provides a schematic drawing of the cutting process with two main characteristics:

- High strain plastic deformation within a shear zone
- Heavily loaded region on chip-tool interface

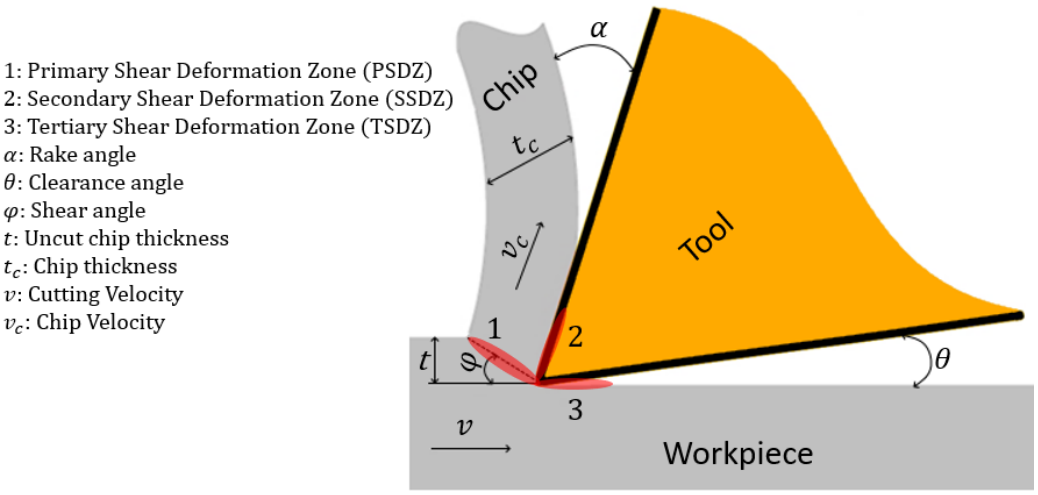

Figure 8. Schematic diagram of a cutting process [based on [20]].

The main characteristics of cutting shown in the diagram (Figure 8) represent the major phenomena occurring at the tool-chip interface [20]. This simplified model highlights the three main regions where plastic deformation occurs: Primary Shear

Deformation Zone (PSDZ), Secondary Shear Deformation Zone (SSDZ) and Tertiary Shear Deformation Zone (TSDZ).

The primary shear deformation zone is a region at which chip formation occurs. Investigations of this region are mostly focused on the characteristics of the material's plastic deformation. Those mechanisms may vary depending on cutting conditions and material composition.

The secondary shear deformation zone is where intense friction develops on the tool rake face, which generates high stresses. This is the main zone of interaction between the tool and the generated chip. In this zone, tool wear is determined by several wear mechanisms (adhesion, abrasion, diffusion, and oxidation). Studies of this region are typically focused on the frictional behavior occurring at the secondary shear zone and along the length of the cutting tool.

The tertiary shear deformation zone is where friction occurs on the surface of a machined part. This is the main zone where surface integrity may vary due to cutting conditions and tool performance. Investigations of this region are focused on surface integrity issue, such as surface roughness and distribution of hardness.

2.2.2 – Machinability of Super Duplex Stainless Steel

Machinability can be defined as the capacity of a metal to be cut, drilled or grinded by tools under predetermined conditions. This capability is represented through a value known as the machinability index, where a set of cutting process variables are combined to compare the performance of different materials. This index value can be a combination of material hardness, elasticity modulus, compressive strength, and other physical and mechanical properties.

Materials that have a high machinability index will most likely excel in the following aspects:

- Tool life performance
- Cutting Forces
- Chip Control
- Surface roughness of machined workpiece
- Material Removal Rate
- Productivity

Machinability (as well as the outcoming machining part) can be affected by other factors of the cutting process, such as:

- Tool characteristics such as nose radius
- Cooling conditions
- Chatter

- Type of cutting process, such as finishing, roughing, etc.

Duplex stainless steel (grade 2507) and super duplex stainless steel are renowned for their poor machinability which regularly involves high cutting forces, high cutting temperatures, short tool life, limited material removal rate and fast work hardening during the cutting process.

Duplex and superduplex grade steels have a particularly poor machinability compared to other stainless steels. The following image compares the machinability indexes of different stainless-steel grades using carbide and high-speed steel cutting tools.

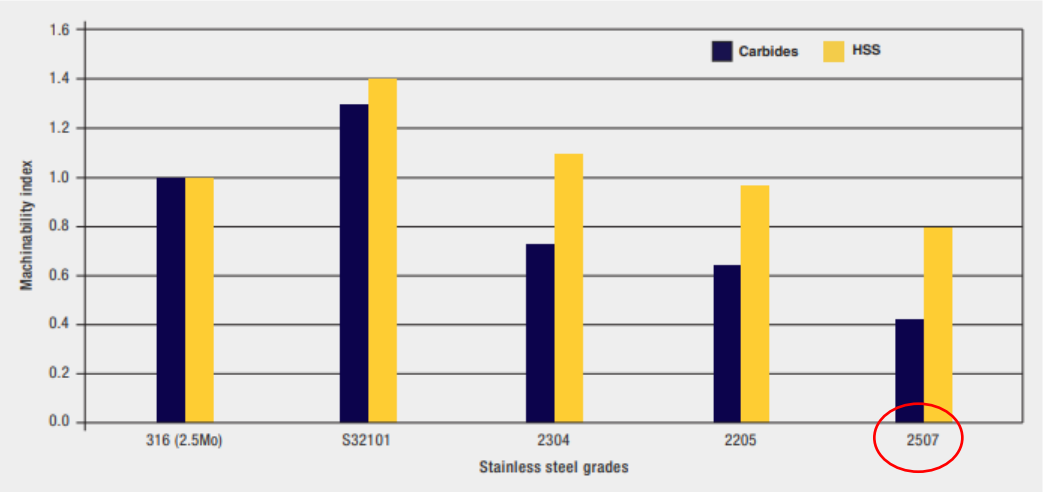

Figure 9. Machinability index on different stainless-steel grades [6].

The defining characteristic of duplex grade stainless steel is its machinability behavior. This material usually produces long and curly chips during machining, which adhere to the cutting tool, form a built-up edge, and eventually break away. This trend

repeats itself several times over the course of a typical cutting session, leading to very poor tool life.

Duplex and super duplex stainless steel have a high tendency of work hardening and poor thermal conductivity, which makes them difficult to machine.

Built-up edge formation typically occurs during the machining of hard-to-cut alloys even at higher cutting speeds, due to their high work hardening and high strength. Chip formation generates high loads, which in turn results in intense cutting forces. High temperatures at the tool/chip interface cause tiny parts of the workpiece to weld to the cutting tool and eventually break away, carrying off a fragment of the cutting tool with them. The unstable cutting process is being driven by adhesion of the workpiece to the tool. The presence of alloying elements (such as nickel and chromium) intended to improve pitting corrosion resistance further contributes to the poor machinability of duplex grade stainless steel. They also increase work hardening and reduce thermal conductivity, thus accelerating tool wear.

The thermal conductivity of duplex stainless-steel grades plays an essential role in their machinability. Due to their chemical composition, stainless steels generally have a low thermal conductivity which leads to a high amount of heat in the material being unable to dissipate within the cutting zone. This promotes chemical-physical reactions during tool-chip interaction, which results in the plastic deformation of the cutting tool during machining.

2.2.3 – Cutting Forces

Trent et al [21] recommends that cutting forces should be studied first as vital indicators of machinability. They also provide information useful for selecting the appropriate workpiece materials, cutting tools, coatings, cutting conditions, types of cutting fluid and other variables such as the instrument's deflection and clamping.

During tangential cut operations such as finish turning, a cutting force (Fc) is produced as a result of workpiece material acting on the surface of cutting tool. Machining typically involves the following force components:

- Cutting Force (Fc) – The main cutting force acting in the cutting direction.
- Feed Force (Ff) – Acts in the longitudinal direction and tends to push the tool away from the workpiece.
- Depth force (Fz) – Usually the smallest cutting force component. [22].

High cutting forces are typically present during the machining of duplex grade stainless steels, due to the elevated plastic deformation and greater contact length between the chip and the tool. In figure 10 a simple schematic drawing of a turning process is shown.

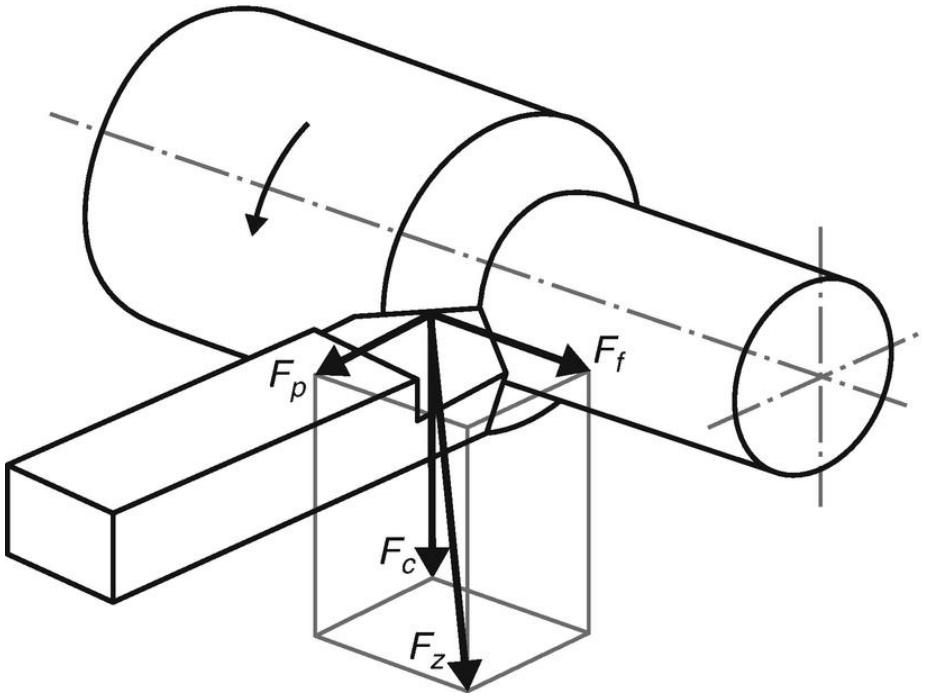

Figure 10. Turning forces direction [used with permission 22].

2.2.4 – Friction in Metal Cutting

Gekonde et al. [23] showed that tribological phenomena at the tool-chip interface can control chip formation process as well as wear resistance. Friction during cutting is affected by the heat generated during machining due to the high sliding velocity and heavy loads present at the tool-chip interface.

In classical mechanics, friction can be defined as resistance to the motion of one object moving relative to another. Under classical tribological conditions, it can be calculated using equation 2. The coefficient of friction (μ) can be expressed as a ratio

between the force necessary (F) to initiate or continue the sliding of an object and the normal force (N) acting on a sliding interface.

$$\mu = \frac{F}{N} \qquad \textbf{Equation 2}$$

During metal removal operations, friction is mainly generated and retained within the secondary shear deformation zone (SSDZ). As the cutting process proceeds, the tool-chip interface can be divided into two main zones: the sticking and the sliding zone [24].

Within the sticking zone, the tool tip becomes attached to the workpiece and will not slide during the shear process. Such behavior is a result of the interaction of various characteristics within the entire system, such as tool material, workpiece material, tribofilm generation, lubricating conditions and cutting parameters, all of which directly affect the tool life, cutting forces and possible wear mechanisms. Figure 9 presents a schematic depiction of process.

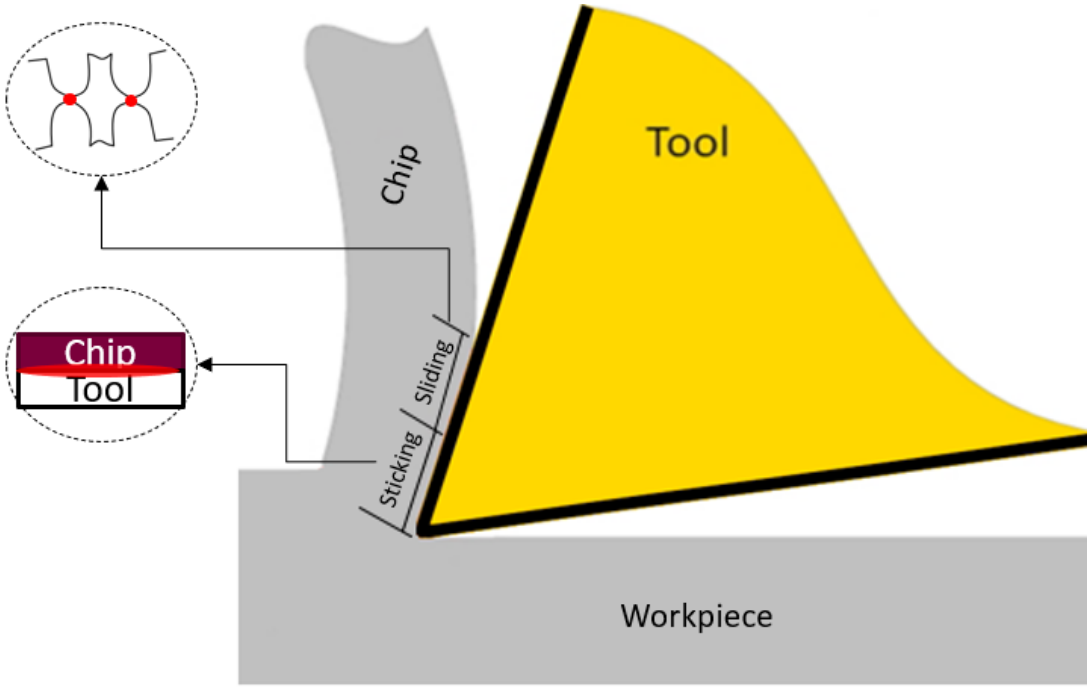

Figure 11. A schematic representation of sticking-sliding zones [based on 23].

2.3 Chip Formation

Studies of the chips generated during the machining process provides useful information about the mechanisms of chip formation and material removal within the cutting zone. A chip can be defined as a portion of material removed during the cutting process with an irregular geometric shape as its main characteristic [20].

The following image shows a schematic diagram of chip formation during the cutting process:

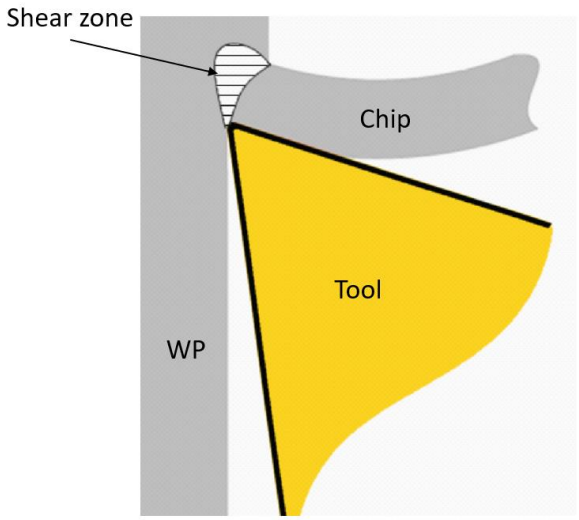

Figure 12. Schematic diagram of a chip formation [based on 20].

Chip formation occurs in a periodic manner during the process of shearing in the following four steps:

- 1st step – During the machining process, the cutting tool moves beneath the depth of cut and the workpiece material begins to elastically deform.
- 2nd step – The workpiece material will reach its yield limit and begin to plastically deform. Plastic deformation continues until it reaches the material's yield limit, when it transforms into the fracture phase.
- 3rd step – The material enters the fracture phase. The region where the material undergoes tensile deformation and fracture is called the shear zone. This process is initialized at the edge of the cutting tool and determines the course of chip formation.

- 4th step – After the material begins to fracture, it will slide along the rake face of the cutting tool, producing a chip.

2.3.1 – Chip types

Shawn et al. [20] classified chips into different types according to material properties such as hardness, yield strength and others, as well as the cutting conditions (feed rate, depth of cut and cutting speed). Whenever a chip slides along the rake face of a tool during the cutting of a ductile material, a continuous chip will likely form, whereas a discontinuous chip will likely result from a fragile material.

Stepheson et al. [19] classified chips into the following types: discontinuous chips, continuous chips (which is the most desirable type), continuous chips with a built-up edge and shear localized chips formed when the material undergoes heavy deformation. These types are depicted in figure 13.

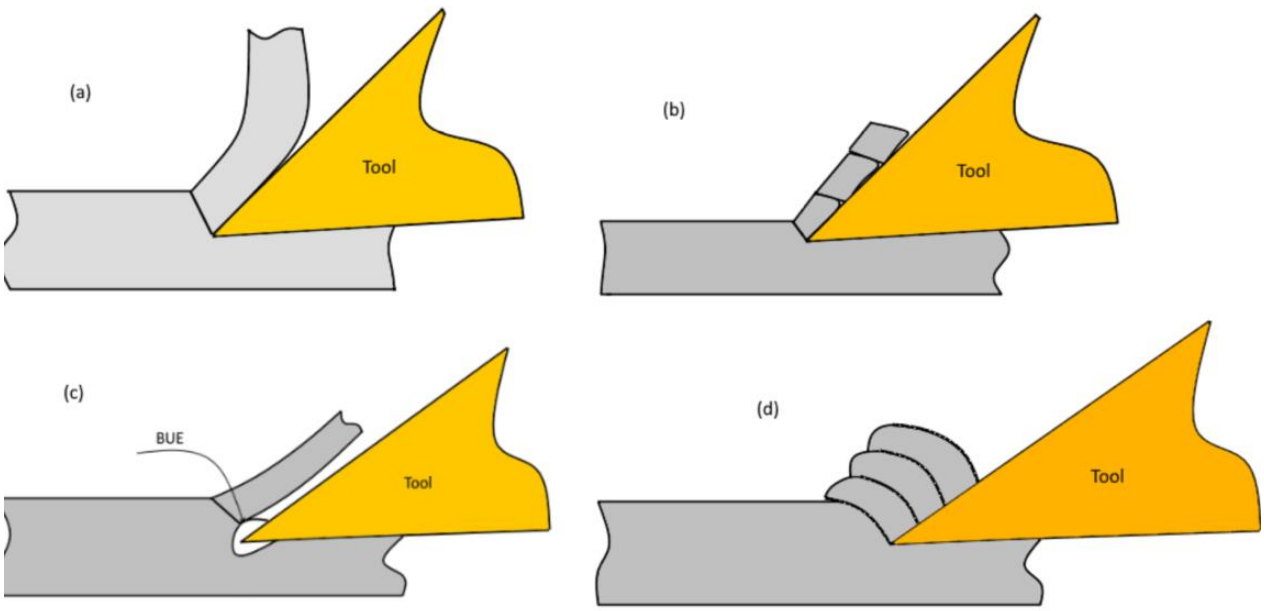

Figure 13. Four chip types: (a) continuous, (b) discontinuous, (c) continuous with built-up edge and (d) shear localized [based on 19].

Factors that may influence chip formation during cutting include the workpiece's properties, tool material, coating, tool geometry, cutting conditions, cooling conditions and other characteristics. These factors will likely affect interactions occurring between the tool-chip interface.

- Discontinuous chip formation is often observed in brittle materials such as beta brass or materials with high yield stresses. This type of chip can also form at low cutting speeds, high feed rate and low rake angle. The detachment of the generated chip typically occurs when the chip fails to

plastically deform. As a consequence, cracks appear at the cutting zone and then propagate, eventually forming a discontinuous chip.

- Continuous chip formation typically occurs in materials with a high ductility and that are usually machined at high cutting speeds, such as low carbon steel, copper, and aluminum. This type of chip is produced in a steady state, without fracture occurring in the shear zone. As such, it is associated with good workpiece surface finish as well as low cutting forces.
- A continuous chip with built up edge formation is formed when a part of the workpiece material becomes welded to the cutting tool. This most often occurs in materials with low thermal conductivity and those which contain alloying elements such as Chromium, Titanium and Nickel. Eventually this structure breaks away and forms once again multiple times during machining. The effects of the built-up edge on the workpiece and cutting tool characteristics will be discussed in the Tool Wear section.
- Shear localized chips become more common as new materials, higher speeds and more robust machines were being implemented in machining. This chip type is characterized by intense shear zones and undergoes total deformation. Furthermore, this type of chip tends to weld due to the intense friction and high temperatures generated during workpiece deformation.

2.3.2 – Sawtooth chip formation

A sawtooth chip is usually generated in materials with quite aggressive plastic deformation, such as stainless steel. Factors that might result in this type of chip formation during the cutting process include the state of the workpiece, tool material, coating, tool geometry, cutting conditions, cooling conditions and others. [20]

2.4 Cutting Tools

New technologies and materials require the implementation of new cutting technologies that aim to increase the material removal rate and as a consequence, improve the productivity and cost effectiveness of machining. Shawn et al [20] states that proper selection of cutting tools for specific applications is a major determining factor of machining process productivity. High temperatures and heavy loads on the cutting tools are expected during machining due to the frictional processes discussed previously. Overcoming these problems would require the cutting tools to possess the following characteristics:

- **Hardness** – The cutting tool's hardness must be superior to that of the workpiece. This is a major factor of influencing wear intensity, especially at high temperatures typical in machining.
- **Toughness** – During machining operations, a cutting tool must be able to absorb energy without being fractured.
- **Wear resistance** – Wear resistance of a cutting tool is directly proportional to its cutting efficiency. This characteristic is associated with its chemical composition as well as the optimized combination of toughness and hardness.
- **Chemical stability** - The cutting tool should not intensively react with the workpiece material.

The set of properties is essential for ensuring the efficiency of the cutting process.

2.4.1 – Residual Stresses

Residual stresses can be defined as the multiaxial static stresses in an elastic body under conditions of mechanical equilibrium which can be present in an isolated component without the application of external force. [25]

During the deposition of thin film coatings on a cutting tool, residual stresses can be produced from different sources, such as the thermal expansion difference between the as-deposited coating and the tool, as well as the kinetic energy of individual particles generated by defects and irregular surface topography. [26]

These residual stresses can have a large impact on the coating's mechanical properties and the ensuing tool life. There exist two kinds of residual stresses, tensile and compressive. Tensile stresses are undesirable once they exceed the elastic limit and lead to crack generation under operation. On the other hand, compressive stresses can increase the number of cycles before the emergence of crack nucleation through the mean stress effect, which is essential for the component's fatigue strength as well as beneficial for the cutting tool's substrate. [27]

2.5 Tool Wear

Selection of appropriate cutting tool materials such high speed steels (HSS), carbides, ceramics, diamond in addition to suitable cutting conditions and workpiece materials will directly affect tool life and wear performance. The cutting tool is exposed to high temperatures and heavy mechanical loads during machining operations. Therefore, intensive tool wear is an unavoidable feature of a cutting process.

Tool life can be defined as the time taken for the tool to reach a failure condition. One such suitable criterion of tool failure is flank wear exceeding 300μm, according to ISO 3685. [28]

A typical tool life curve presents three distinct zones:

I. Rapid initial wear, where the cutting tool tip is initially blunted. This can occur during the very first passes.

II. Steady state wear, with a relatively slow wear rate.

III. Rapid wear growth prior to failure, followed by, severe tool wear until the end of tool life. [29]

Tool life curve can be characterized either by machining time or cutting length. An example of a generic tool life curve is given in figure 14.

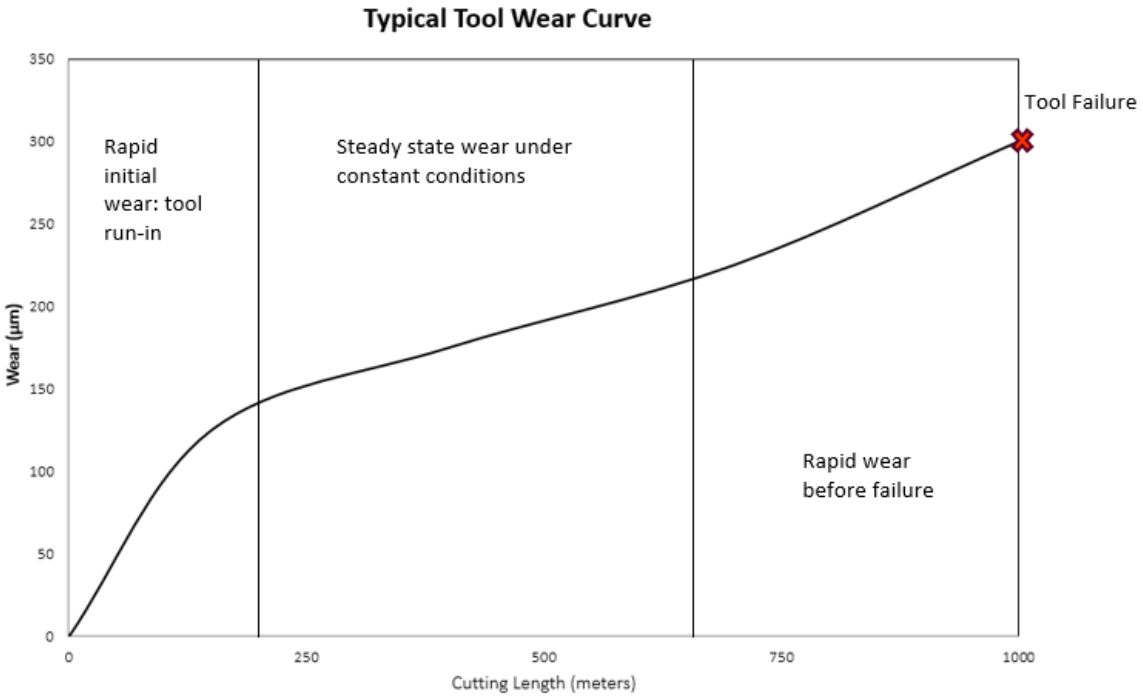

Figure 14. An example of a typical tool wear curve [based on 29]

2.5.1 – Types of wear mechanisms

Stephenson et. Al [19] has classified tool wear into four main categories. They are:

- Abrasive wear when hard particles within the workpiece affect the surface of the tool. This is the most common type of wear during machining.
- Adhesive wear caused by the chemical interactions between the interacting materials during friction. This type of wear can lead to built-up edge formation as well as poor tool life, poor surface finish and dimensional accuracy of the workpiece.

- Diffusion wear, which is driven by high temperature generated at the tool/chip interface, leads to interdiffusion of the workpiece and cutting tool material. One of diffusion's possible outcomes is crater wear on the rake face of the cutting tool.
- Oxidation wear caused by the chemical reaction of the worn cutting tool and the workpiece material with atmospheric oxygen.

2.6 Coating in Cutting Tools

Hard thin films coatings have been largely used for metal forming, die casting, injection molding and machining in recent years. These coatings possess the following beneficial properties: low thermal conductivity, low friction and high wear resistance. As of today, most machining tends to be conducted at a high cutting speed, without coolant and with higher material removal rate for hard-to-cut materials, which makes such properties highly desirable in industry. Application of coatings on cutting tools still presents one of the best methods for improving the machining performance.

Coatings provide the tool with the following beneficial properties:

- Ability to conduct cutting operations with no coolant (dry cut).
- Wear resistance improvement.
- Enhanced heat dissipation.
- Reduction of friction.
- High operational cutting speed and material removal rate.
- Capability of reducing or altogether eliminating the built-up edge.
- Reduced flank and crater wear intensity.

Optimal coating performance results from a combination of mechanical (beneficial stresses, wear resistance, hardness) and physical (chemical stability, adhesion to the substrate) properties at both room and elevated temperatures.

2.6.1 – Types of coatings

When cutting tools are properly coated in accordance with machining conditions such as workpiece material characteristics and cutting parameters, this can considerably improve tool life as well as expedite dry machining and material removal rate, resulting in a higher productivity. The main advantages provided by coating application on cutting tools are the improvement of wear resistance, fatigue, and oxidation resistance as well as the reduction of thermal shock.

The deposition of coatings capable of generating thin tribo-films on the cutting tool can be divided into two main categories:

- Chemical Vapour Deposition (CVD) performed at high temperatures (~1000°C) inside a vacuum chamber.
- Physical Vapour Deposition (PVD) performed at lower temperature (~450°C), inside a vacuum chamber from a source (target), to the substrate. [30]

Although both of these methods offer distinct advantages, Physical Vapour Deposition is a newer technique that has seen more widespread use in recent times, especially for the application of thin films coatings.

The most commonly used method of Physical Vapour Deposition is the arc method, which consists of an electrical power source hitting the cathode (target) and transforming the target material from a solid to a liquid or gaseous (ionized) state, dragging to an anode

(+) substrate material through application of an arc current and/or bias voltage. This method can reduce the target material state into tiny droplets that can then be deposited on the surface of a tool. [30,31] Figure 15 illustrates how a PVD process works.

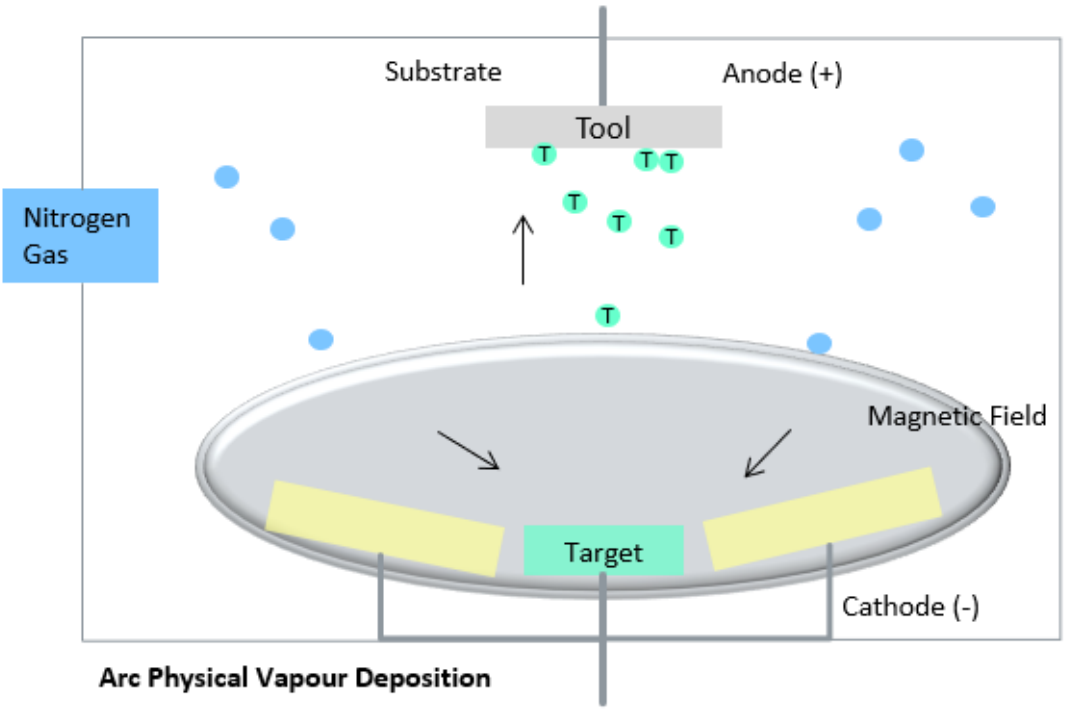

Figure 15. A schematic drawing of a PVD process [based on [31]]

2.6.2 – Tribofilms in coatings

During cutting operations, intense friction is generated due to the relative movement between the chip and the tool. The generated mechanical loads and temperatures can break the bonds in the materials, resulting in atomic transfer to the friction surfaces and their interaction with the external environment. [32] A coating applied on a cutting tool can be useful in these situations since its outer layers can chemically react with oxygen to generate

thin (nano-scale) tribofilms [Fox-Rabinovich and Totten], which possess lubricious/thermal barrier properties.

A typical example of the outlined phenomenon is produced by the commonly available Aluminum-Titanium-Nitride (AlTiN) coating, which thermically reacts with the environment to generate thermal barrier Al_2O_3 films that improve tribological conditions as well as wear resistance of the tool.

2.6.3 –Multi-layer coatings

Properties of cutting tools can be improved when one or more hard thin layers of different compounds such as Chromium Nitride (CrN), Titanium Nitride (TiN) and Titanium Diboride (TiB_2) are combined. Application of such coatings on traditional cutting tool materials can results in an improved tool life.

An optimal combination of different coatings could offer distinct advantages, such as improved adhesion, reduced wear rate, elimination of microcracks, reduction of friction, and eventually, superior wear resistance. The following figure outlines the schematic structure of a multi-layered coating.

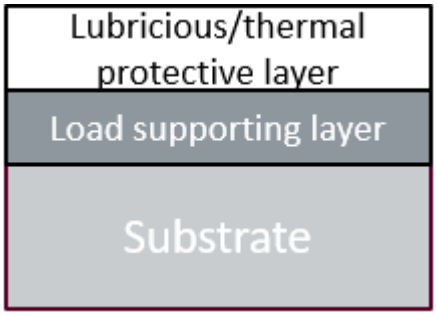

Figure 16. Diagram of a multi-layered coating applied in a cutting tool with different properties. [based on 33]

2.6.4 – Lubricious/thermal barrier properties of the coatings

The coatings applied on a cutting tool can be engineered to address issues during machining and generate a lubricious/thermal barrier tribo-layer. Several processes take place during cutting:

- Spontaneous material transfer to the surface
- De-composition of the coating layer
- A non-spontaneous non-equilibrium process associated with the formation of tribo-oxides on the friction surface. [33]

In modern machining, increased process productivity will inevitably generate a greater amount of heat due to friction. One feasible method of addressing this issue is to apply a coating with lubricious/thermal barrier properties on the cutting tool.

Recently introduced coatings such as Titanium Diboride (TiB_2) or traditional Chromium Nitride (CrN) can form protective tribofilms during the machining operation [34]. These tribofilms play an important role in reducing friction, heat, as well as mitigate built-up edge formation. [33], [35]

Figure 17 presents a schematic drawing of the cutting process with two main sticking and sliding zones and shows how a lubricious tribo-oxide can act to reduce heat within the sticking zone during machining.

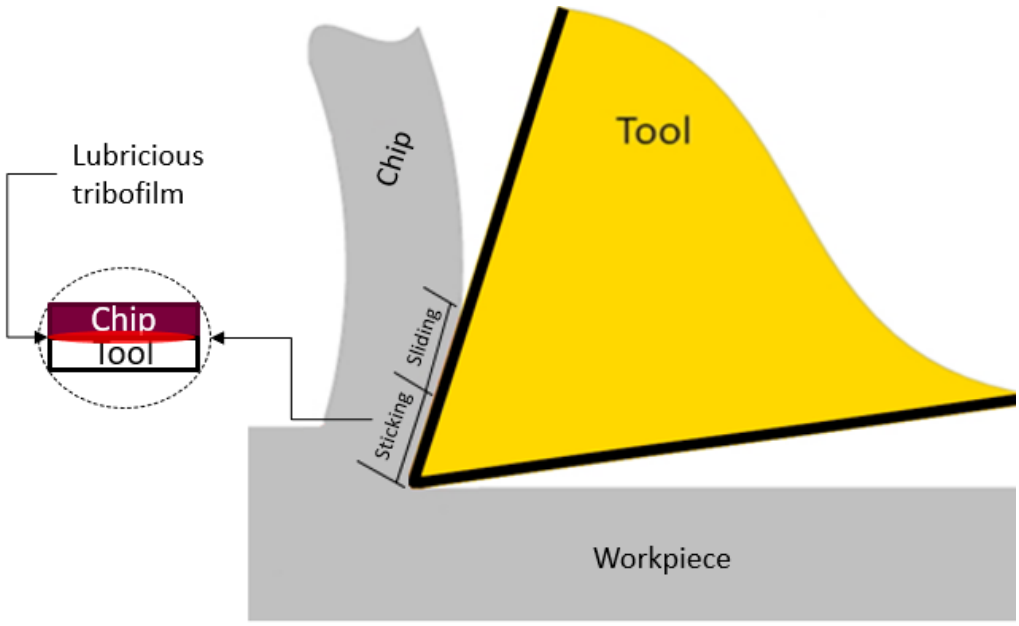

Figure 17. Schematic drawing of a lubricious tribofilm acting in sticking zone during cutting process [based on 34]

2.6.5 – HiPIMS Technology

New workpiece materials, especially with high Nickel content, belong to the category of hard-to-cut adhesive materials. During machining, they tend to cause intense adhesion with the tool material.

Since physical vapor deposition (PVD) is the most widely used method of applying hard thin film coatings onto the cutting tools, there is an increasing demand for improving this technique as new workpiece materials are being introduced and industries strive to increase the productivity of the machining process. A new and promising (PVD) deposition technology for cutting tools is the High-Power Impulse Magnetron Sputtering (HiPIMS) technique, which enables more precise control over the ionization rate of the sputtered material, as well as a higher ion flux. [37]

Regular plasma-assisted physical vapor deposition can provide different degrees of adhesion of the coating to the cutting tool substrate, varying the levels of residual stresses as well as the formation of droplets that could lead to poor tool life. [38]

Figure 18 presents a schematic comparison between traditional plasma-assisted physical vapour deposition and High-Power Impulse Magnetron Sputtering (HiPIMS) techniques.

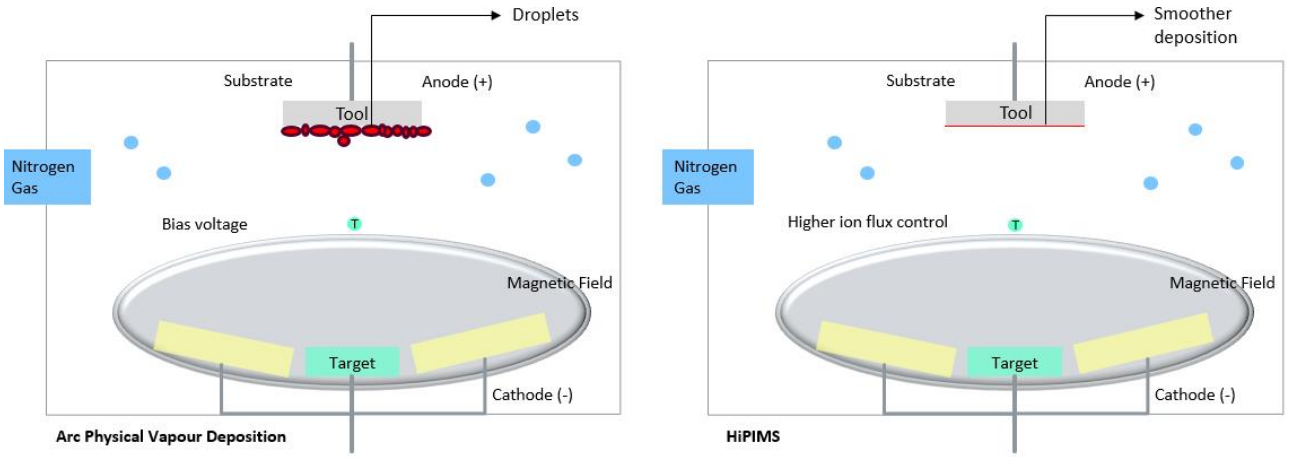

Figure 18. Schematic comparison between arc PVD and HiPIMS coating deposition [based on 38].

2.7 State of art

The biggest problem during the machining of Super Duplex Stainless Steel is posed by very aggressive tribological conditions. Cutting tool coatings need to both overcome the potential machining issues of hard-to-cut materials and be capable of increasing tool life. However, their performance is substantially dependent on the deposition techniques, chemical composition of the coating layer, as well as their mechanical properties. Recent studies investigating wear performance during the machining of SDSS have shown that high temperatures combined with significant loads accelerate tool wear and considerably hinder tool life. [3], [4], [8]

Paiva et al. [39] conducted a machining experiment on SDSS and evaluated the wear performance of two monolayer Physical Vapour Deposition coatings and one multi-layer Chemical Vapour Deposition coating. Yassmin et al [8] studied built-up edge formation on the cutting tool during SDSS machining under finish turning conditions.

The latest generation of Physical Vapour Deposition, also known as High Power Impulse Magnetron Sputtering (HiPIMS) has shown promising results by providing superior control of the deposition process as well as improving coating adhesion. Chinchanikar, et al. [40] conducted a machining experiment on AISI 4340 and evaluated its wear behaviour during a turning operation under dry and minimum quantity lubrication (MQL) conditions. This study employed three distinct coatings deposited by a HiPIMS technique. At the same time, Li, et al. [41] studied microstructure as well as the mechanical properties of the multi-layer HiPIMS coating during the machining of Inconel 718.

The contribution of the current research is a complement to the previous here described, since the usage of bi-layer HiPIMS coating applied on cutting tool during machining of Super Duplex Stainless Steel has not yet related to its tool life performance.

CHAPTER 3 – METHODOLOGY

This chapter presents the experimental methodology used in this study. The experimental procedure was designed to address the aforementioned issues during machining of Super Duplex Stainless Steel. A schematic diagram highlighting the steps of the experimental study is shown in figure 19.

The first step of this study consisted of workpiece characterization, microstructure analysis and the calculation of a theoretical PREn number.

The second step was an experimental procedure in which a mono-layer coating and multiple bi-layer coatings were applied on cutting tools. The resultant machining data concerning adhesion, residual stresses, architecture characterization, topography as well as micromechanical data such as microhardness, elastic modulus, and fracture toughness were collected and studied.

Tool life performance was analysed in the third step. Tool life and cutting force data were collected and tool wear characterization was performed.

Lastly, chip analysis was carried out to investigate the outcome of Super Duplex Stainless Steel machining. This analysis evaluated the microstructure of the workpiece material, micro-hardness, and topography.

The experimental procedure was also divided into two phases. The first phase of the machining experiment was performed under the typical finishing conditions

(Experiment A) recommended in literature. The second phase was conducted under more severe conditions present at elevated cutting speeds (Experiment B).

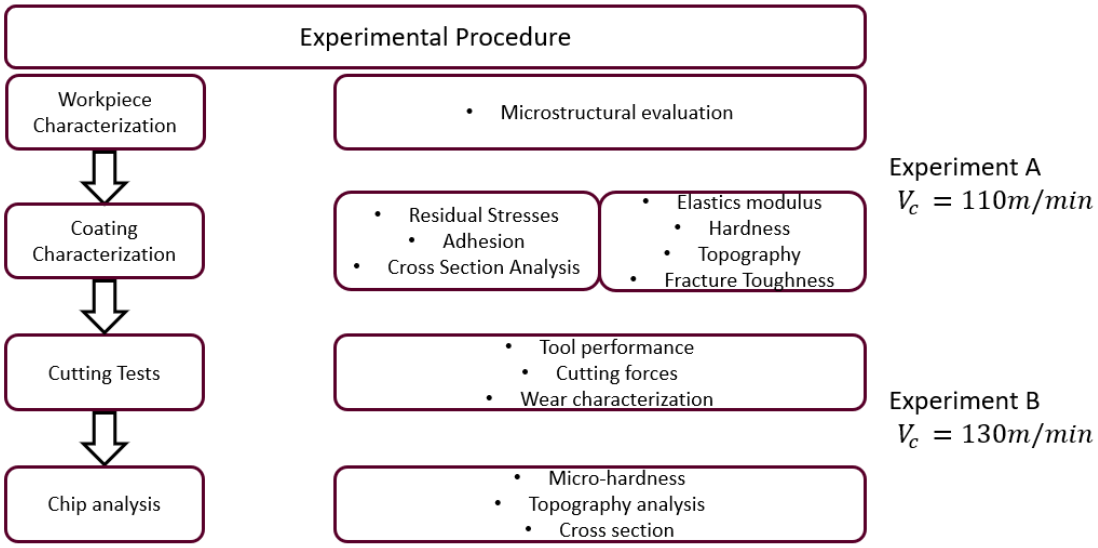

Figure 19. Schematic diagram of experimental procedure.

3.1 Workpiece Characterization

The workpiece material used throughout this study was Super Duplex Stainless Steel UNS 32750, a manufactured tube with dimensions shown in Figure 20, produced by Vallourec Tube Solutions of Brazil.

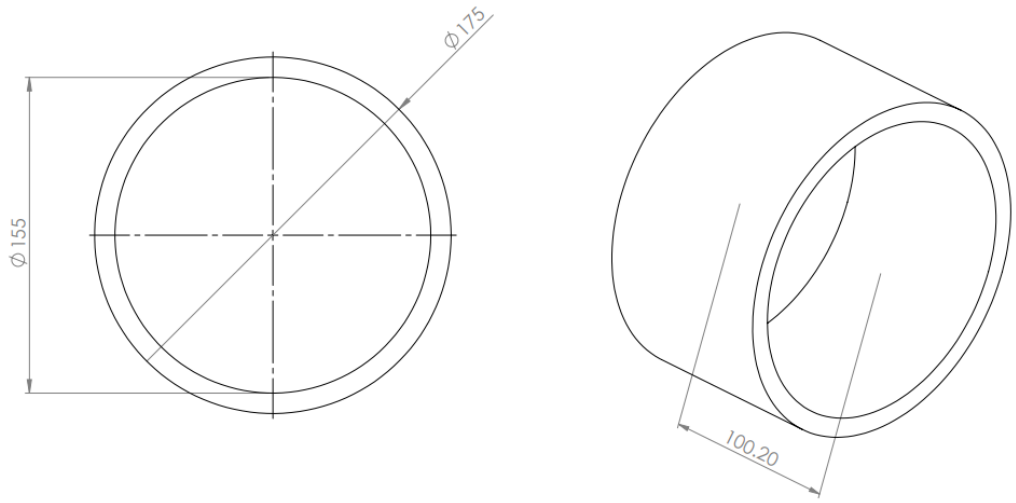

Figure 20. Workpiece material dimensions.

This is the same workpiece material used in petrochemical applications. The chemical composition of the workpiece material given by the supplier is shown in table 5 below.

Table 5. Chemical composition of Super Duplex Stainless Steel UNS 32750 (Vallourec)

Element	Cr	Mo	N	Ni	C	Mn	Si	Cu	P	S	Fe
Weight (%)	25	4	0.3	7	0.03	1.13	0.65	0.78	0.0012	0.018	Balance

According to the data provided, it is possible to estimate the pitting resistant equivalent (PREn) of the workpiece material SDSS UNS 32750 in Equation 1. The estimated pitting resistant equivalent is:

$$PREN = \%Cr + 3.3\%Mo + 16\%N$$

$$PREN = 25 + 3.3\%*4 + 16\%*0.3$$

$$PREN = 43$$

The value of the workpiece material's Pitting Resistant Equivalent number classifies it as a SDSS, according to the NACE MR1075 standard – which requires PREn to be no lower than 40 in this type of material.

To analyze the microstructure, a small amount of workpiece material was cut parallel to the axial direction of the tube and then mounted in epoxy resin, polished according to conventional metallographic procedures and etched in an *aqua regia* solution – a mixture of Hydrochloric Acid (HCl) and Nitric Acid (HNO3) at a molar ratio of 1:3.

To analyze the microstructure of the workpiece and discern the nature of each phase, images from the etched sample were acquired under a Keyence VHX-6000 optical

microscope using a 1000x lens. Afterwards, the distribution of austenite and ferrite phases was determined using Fiji software, as given in figure 21.

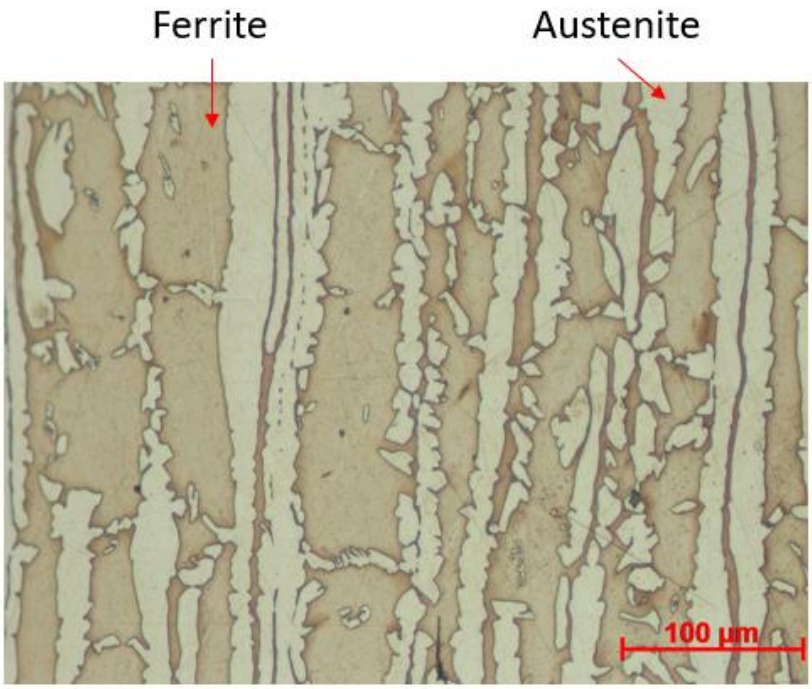

Figure 21. Workpiece material microstructure phases.

Software analysis reveals a well-balanced microstructure consisting of roughly 48% austenite and 52% ferrite.

3.2 Coating Characterization

3.2.1 – Residual Stresses

Surface residual stresses of the coating were measured on WC-Co polished samples by an X-Ray Diffractometer using a Titanium target at a power of 30kV and 20mA. The X-Ray Elastic constant was fixed at 12,200ksi, Bragg angle (2θ) at 80º. 20 measurements were performed for each sample.

3.2.2 – Adhesion

Coating adhesion was measured on WC-Co polished samples by an AntonPaar RST-3 Revetest Scratch Tester. A 200μm radius diamond Rockwell AJ-259 indenter was used to perform the scratch test. The test was performed in a 3-scan procedure progressive mode, in which the initial pre-scan of surface topography was followed up by a progressive scratch scan where the load was gradually ramped up from 0.5N to 150N at a length of 3mm. Finally, a post topography scan was performed. Three scratch tests were carried out for each sample to account for the variability of results.

3.2.3 – Elastics Modulus & Hardness

Micromechanical data (elastics modulus & nanohardness) of the coatings was collected from WC-Co polished samples at room temperature by an AntonPaar MicroMaterials NanoTest P3 system. Following the standard procedure ISO 14577-4, a diamond Berkovich B-V 76 indenter calibrated in terms of shape, displacement, load and frame compliance was used to perform the test. The maximum load of the test was set to

be 100mN. This load was chosen to ensure an accurate measurement of the thin coating films' contact depth and minimize the possible interference of the sample's surface roughness. Fifteen indentations were measured for each sample. Furthermore, the relationship between hardness and elastics modulus was also calculated.

3.2.4 – Surface Topography

Surface topography of the coatings was performed through Atomic Force Microscopy on WC-Co polished samples at room temperature with vibrational stability being ensured by AntonPaar AFM Tosca-400 equipment. A probe was connected to a cantilever that scanned the surface topography.

Surface roughness measurements were taken according to ISO 25178 Three surface topography scans were performed for each sample.

3.2.5 – Fracture Toughness

The fracture toughness of WC-Co polished samples was assessed at room temperature using an AntonPaar RST-3 Revetest Scratch Tester. Following the standard procedure that involved the Palmqvist toughness method (ISO 28709), a diamond Vicker indenter V-K 81 was used to conduct the test with the load varying from 100-150N. Coating toughness was then calculated from the relationship of the load to the total length of the cracks – or in other words, from the center of indentation to the crack tip. Five indentations were measured for each sample.

3.2.6 – Cross Section Analysis

Cross Section Analysis of the coatings was performed by cutting the samples in half by an electrical discharge method from the top to the bottom, so as to not damage any of the studied coating layers.

Images of the ensuing state were then acquired using Scanning Electron Microscopy – TESCA Vega II equipment.

3.3 Cutting Tests

A study of machining performance was conducted during a turning operation using a Nakamura-SC450 lathe as shown in figure 18, under the following conditions: (i) Feed Rate: 0.15mm/rev, (ii) depth of cut: 0.5mm, (iii) 6% fluid coolant (iv) cutting speed: 110m/min (experiment A) and 130m/min (experiment B).

These conditions were used to machine SDSS and observe its resulting tool life performance and cutting forces. The tests were conducted in cutting length passes that varied from 150-200m and the tests were repeat three times with similar behaviour. Cutting force data were collected by a quartz dynamometer Kistler 9121 connected to the tool holder, three-orthogonal components of force (F_c, F_f and F_z), measurement ranges of -3kN and 3kN in three (X, Y and Z) directions and a natural system frequency of 10kHZ.

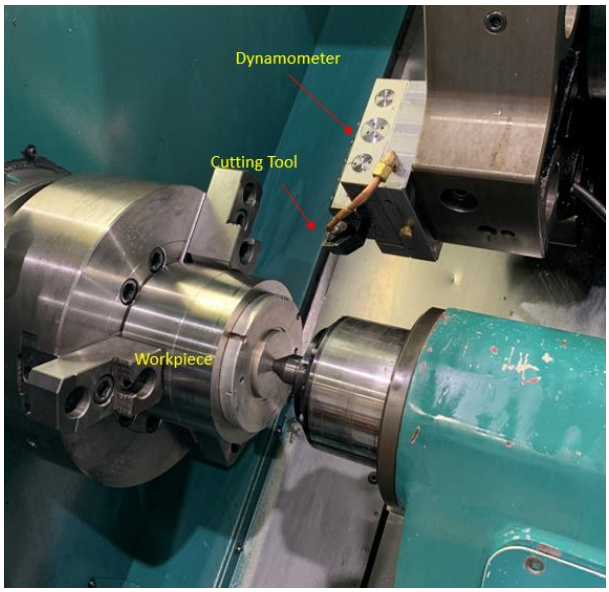

Figure 22. Machining Setup

The cutting tool used in this machining operation was a carbide turning finishing insert manufactured by Sandvik, model CNMG120408-SM-H13A. A combination of Bi-layer coatings cconsisting of an AlTiN layer deposited on the bottom by Oerlikon-Balzers and top layers of TiB_2, WC/C, CrN and AlCrN deposited by HiPIMS was selected due to its properties (lubricious, thermal barrier, load support) to be used in two experiments alongside a mono-layer commercially available AlTiN coating deposited by Oerlikon-Balzers and the uncoated tool. Coating composition and architecture are presented in table 6.

Table 6. Selected Coatings, Composition and Architecture

Coating	Composition	Architecture
AlTiN	$Al_{67}Ti_{33}N$	Monolayer
AlTiN + TiB_2	$Al_{67}Ti_{33}N/TiB_2$	Bi-layer
AlTiN + WC/C	$Al_{67}Ti_{33}N$/WC/C	Bi-layer
AlTiN + CrN	$Al_{67}Ti_{33}N$/CrN	Bi-layer
AlTiN + AlCrN	$Al_{67}Ti_{33}N$/AlCrN	Bi-layer

The cutting operation was divided into two different experiments – the first experiment A served as a benchmark of machining behavior and the second experiment B was designed to increase the material removal rate (higher cutting speed) based on results acquired from experiment A.

Experiment A ($V_c = 110 m/min$):

- Uncoated tool
- AlTiN - Commercially available coating
- AlTiN + TiB_2
- AlTiN + WC/C

Experiment B ($V_c = 130 m/min$):

- AlTiN - Commercially available coating
- AlTiN + TiB_2
- AlTiN + CrN
- AlTiN + AlCrN

The selection failure criterion was either 300μm of flank wear/chipping according to ISO 3685 or total machining length of 5000 meters. The wear was measured on a Keyence VHX-6000 Microscope under 200x magnification.

Furthermore, wear characterization was performed using a Scanning Electron Microscope – TESCA Vega II for both experiments.

CHAPTER 4 – RESULTS AND DISCUSSIONS

The following chapter presents the results based on the experimental plan outlined in figure 16. The cutting tests were conducted at the following cutting speeds: experiment A ($V_c = 110 m/min$), experiment B ($V_c = 130 m/min$).

Material removal rate (MRR) is a direct measure of productivity – the greater it is, the more efficient is the machining process. The following equation demonstrates that cutting speed (V_c), feed rate (f) and depth of cut (d) is directly proportional to a higher removal rate during turning operations.

$$MRR = V_c \, f \, d \qquad \textbf{Equation 3}$$

4.1 Coating Characterization

The coating's physical properties determine its performance under high frictions and aggressive mechanical loads present in machining.

Scanning electron microscopy (SEM) images illustrated the architecture and thickness of the coatings, figure 23. Micromechanical and residual stresses data were also collected, with results shown in table 7.

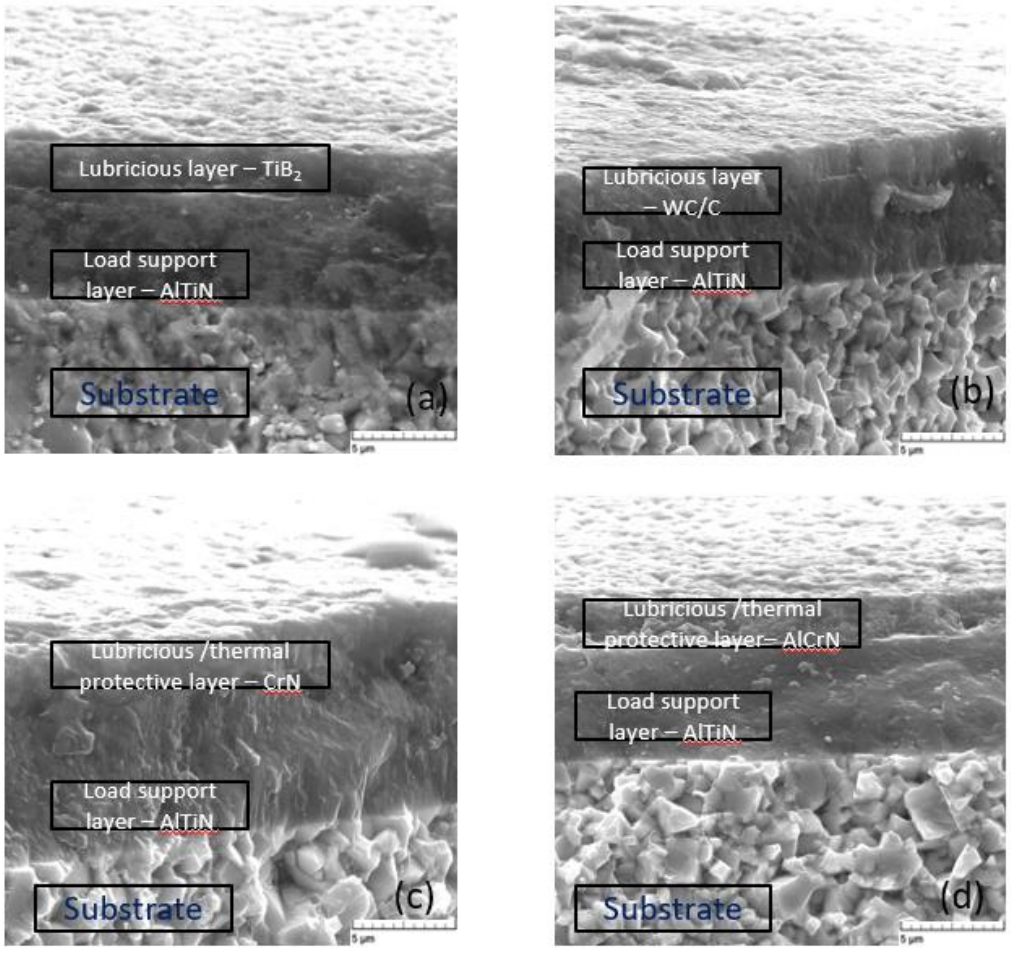

Figure 23. Cross Section Coatings: (a) AlTiN + TiB_2, (b) AlTiN + WC/C, (c) AlTiN + CrN and (d) AlTiN + AlCrN.

Table 7. Architecture of selected coatings and micromechanical data

Coating	Architecture	Thickness (μm)	Hardness (GPa)	Elastic Modulus (GPa)	H/E ratio	Residual Stresses (GPa)
AlTiN	Monolayer	3.88 ± 0.19	35.22 ± 2.87	459.91 ± 24.85	0.076	-1.235 ± 0.11
AlTiN + TiB_2	Bi-layer	7.75 ± 0.12	16.69 ± 2.14	441.59 ± 42.39	0.037	-1.12 ± 0.07
AlTiN + WC/C	Bi-layer	5.54 ± 0.15	13.98 ± 3.59	265.68 ± 56.825	0.052	N/A
AlTiN + CrN	Bi-layer	6.4 ± 0.12	16.99 ± 1.11	379.27 ± 22.77	0.044	-1.834 ± 0.09
AlTiN + AlCrN	Bi-layer	5.67 ± 0.14	30.24 ± 4.27	416.51 ± 49.41	0.072	-3.661 ± 0.14

Unlike other bi-layer combinations, the AlTiN benchmark monolayer coating forms a hard coating thin-film, as well as compressive residual stresses.

Hard coatings tend to be brittle, which can hamper their adhesion to the cutting tool substrate. Lower hardness coatings are desirable for SDSS machining due to their lower shear strength, which can reduce temperature at the tool-chip contact interfaces (sticking-sliding region).

All coatings exhibited negative residual stresses, indicating that all of them were compressive. However, the structure of the bi-layer AlTiN + WC/C coating can not be determined since it appears to be amorphous. X-ray diffraction experiment can only acquire data when the coating has a crystalline structure, which is not the case in the WC/C coating. Residual stresses of the coatings have been studied by different authors [35], [36] and [37]. These stresses are generated during the deposition process where they tend to equalize the forces and geometric compatibility between the coating and substrate.

The compressive residual stresses will be then generated in order to maintain static equilibrium before plastic deformation.

The ratio between hardness and elastic modulus [43] can be used to evaluate tool performance and consequently, the wear resistance of a material. The magnitude of the H/E ratio can be proportional to wear resistance. This process is combined with other factors during machining. Data acquired shows that the the AlTiN + AlCrN bi-layer coating is capable of fulfilling this requirement.

In addition to architecture and micromechanical data, surface topography analysis was performed by Atomic Force Microscopy (AFM) to assess the distribution of roughness throughout the coatings' surface. The results are shown in figure 24.

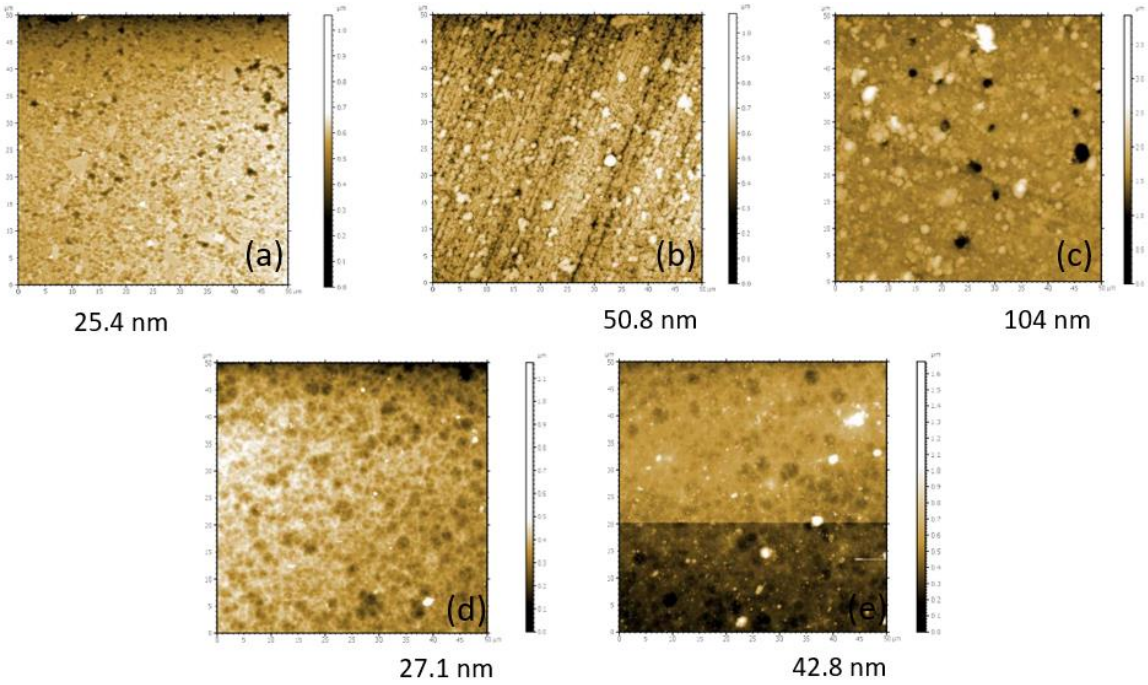

Figure 24. Surface Roughness of coatings: (a) AlTiN, (b) AlTiN + TiB_2, (c) AlTiN + WC/C, (d) AlTiN + CrN and (d) AlTiN + AlCrN

Tiron et al [42] has stated that the HiPIMS PVD coating deposition technique produces lower surface roughness compared to other methods of coating deposition. This can be attributed to the enhanced ion flux being less likely to generate droplets on the surface of the substrate during deposition. However, results from Atomic Force Microscopy experiments show that HiPIMS bi-layer engineered coatings have a rougher surface compared to that of the AlTiN monolayer benchmark coating. One possible cause for this is an already deposited thin coating layer which reacts with the one on top during deposition. The AlTiN +WC/C bi-layer combination has the roughest surface, whereas AlTiN + CrN has the smoothest.

Authors [43], [44] have reported that surface roughness is directly related to the interlocking of mechanical and chemical atomic bonds between the substrate and coating and should be held in account when coating performance is tested.

A scratch test was performed the evaluate the coatings' adhesion and its distribution. The results are shown in figure 25.

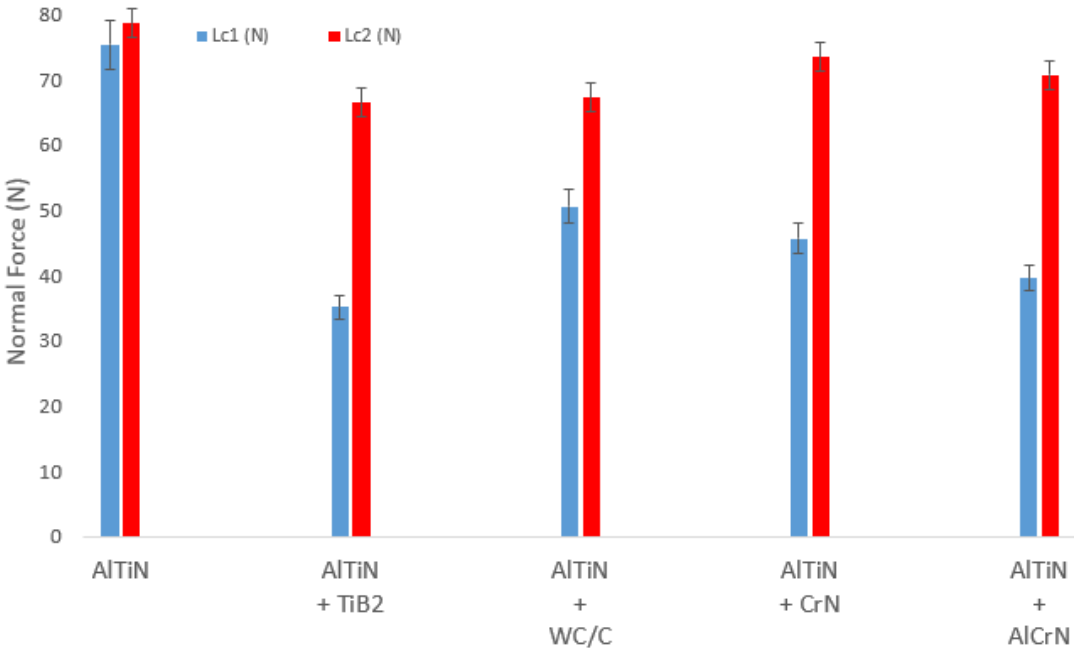

Figure 25. Coating's adhesion.

Chowdhury et al [45] has stated that a scratch test presents an effective way of analyzing the response of the coating under load and can also be used to investigate micro-cracking within the surface/substrate coating layers. Lc1 comes first and it describes the condition at which adhesion failure takes place and the substrate is exposed for the first time, whereas Lc2 comes after, when the coating is completely detached, and the entire substrate is exposed. In general, HiPIMS PVD ensures superior coating adhesion for reasons discussed previously. [38], [45].

Results of the scratch test experiment show that the commercially available AlTiN monolayer features higher coating adhesion. This may be because the deposition of the monolayer coating is less likely to face any interference, whereas a bi-layer coating will

react with the already deposited coating and the substrate, thereby worsening its adhesion. However, it is also possible to observe high adhesion yields in bi-layer AlTiN + CrN and AlTiN + AlCrN coatings. The presence of CrN in the composition of the coatings has been reported to improve adhesion due to its strong alloyability with other materials. [46]

A toughness test was also carried out for all coated tools, with results listed in figure 26.

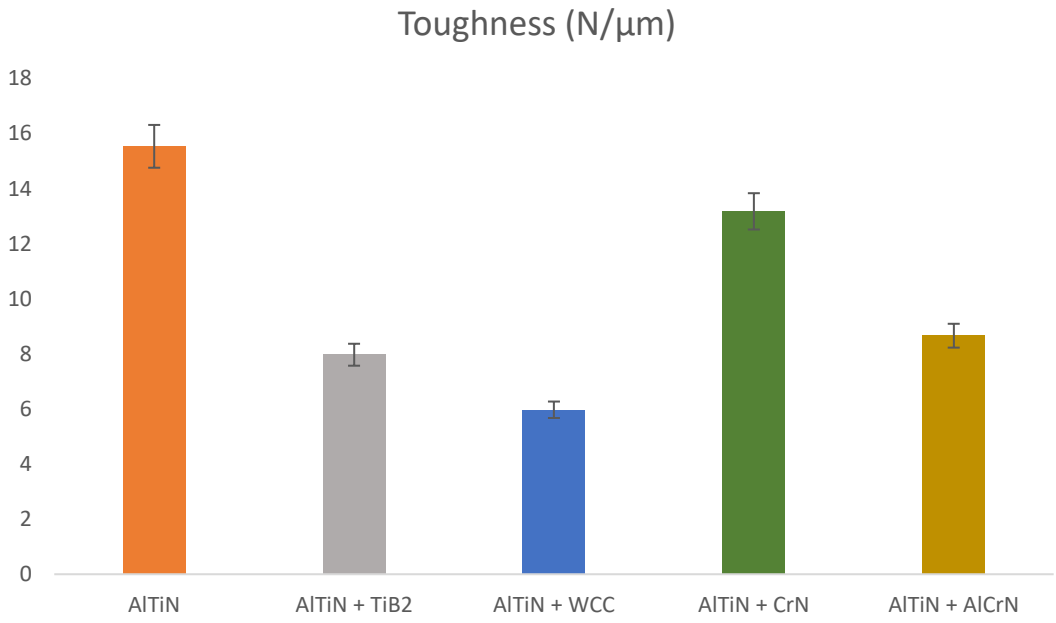

Figure 26. Toughness of coatings.

Authors [44, 47] have described toughness as an indicator of the coating's ability to resist and absorb energy during stress, to delay fracture and avoid cracks. During machining, friction wear can easily propagate and generate cracks under the surface of the coating, which will reduce tool life. The results of the toughness test show that

commercially available AlTiN has the highest toughness out of all the coatings. Coatings containing CrN also have a higher toughness than those without it.

4.2 Performance Evaluation Tests

4.2.1 – Experiment A – $V_c = 110 m/min$

Tool life performance of three coated tools, including one monolayer and two bi-layers, as well as an uncoated tool was tested under finish turning operations listed in section 3. The life curves of the selected tools are depicted in figure 27.

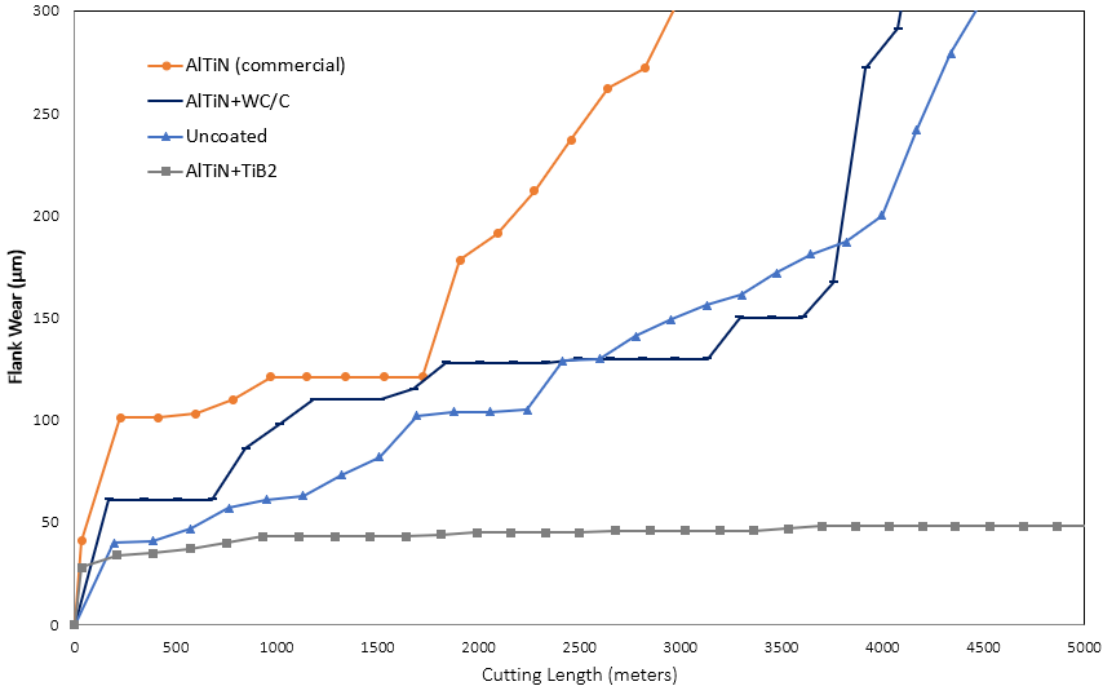

Figure 27. Tool life results given by flank wear versus cutting length (meters).

In this figure it is possible to observe that the AlTiN + TiB_2 bi-layer has the best performance among all the tested tools. This combination experiences negligible damage in comparison with AlTiN + WC/C and the commercially available monolayer AlTiN

which features a short steady state wear followed by rapid wear prior to failure, whereas the uncoated tool underwent progressive wear until it reached the failure criteria.

In addition to tool life curves, the cutting forces of each respective coating were recorded at cutting lengths of 300, 1000 and 3000m (or last pass before failure). The results are shown in figure 28.

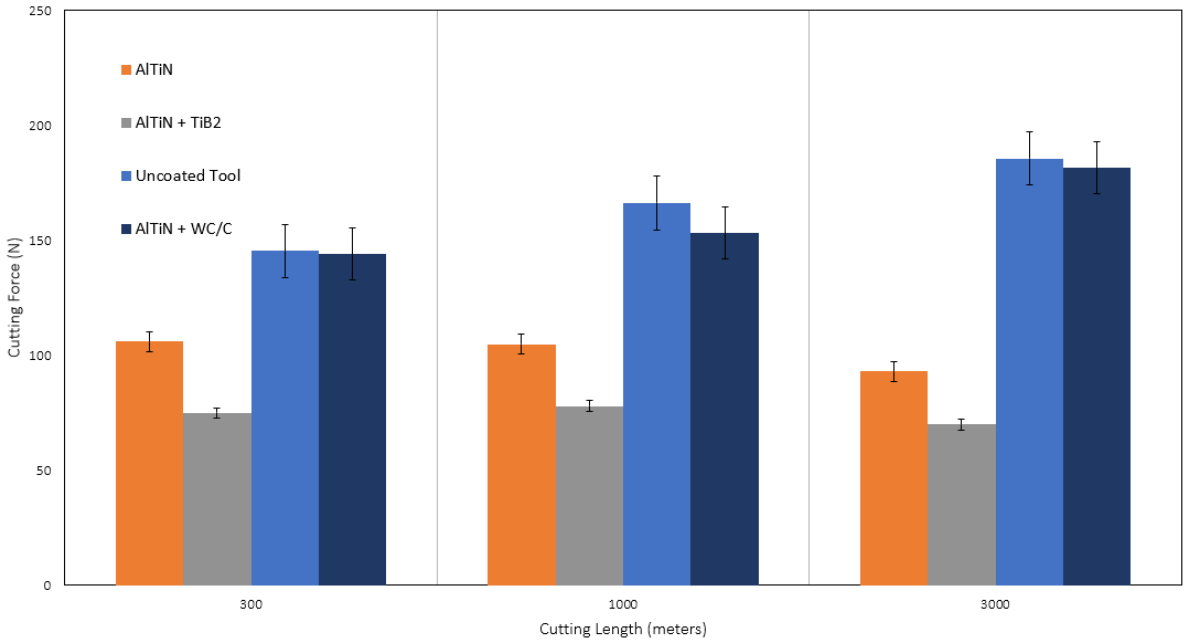

Figure 28. Cutting Forces data from experiment A

Cutting forces data reveal that the uncoated tool and the AlTiN + WC/C bi-layer experience the highest machining tangential forces.

As described by Junior et al. [4], the high mechanical strength of duplex and super duplex stainless steel usually requires more energy for chip removal due to its high mechanical strength, which results in a cutting force increase. This will in turn, cause

more friction to be generated during machining, which further shortens the tool's life. Multiple studies describe the relationship between cutting forces and tool life. [4]

The AlTiN + TiB_2 coated tool exhibits the lowest cutting forces in comparison with the other coated tools. In this case, a Boron Oxide (B_2O_3) lubricious tribofilm may diminish BUE formation, thereby reducing the cutting forces and extending tool life, as reported by several authors. [34]

Scanning electron microscopy images shown in figure 29, illustrate the wear mechanisms of each tool's failure.

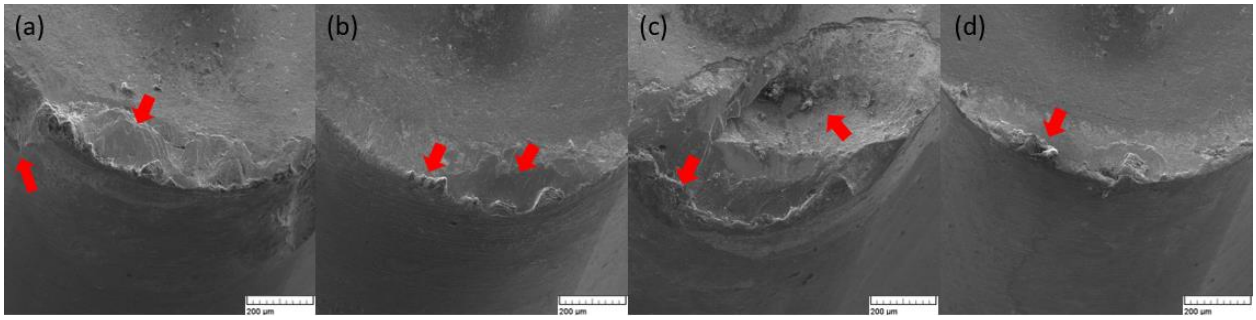

Figure 29. Worn turning tools SEM analysis: (a) Uncoated Tool, (b) AlTiN, (c) AlTiN + WC/C and (d) AlTiN + TiB_2.

The bi-layer coatings in parts (a) and (b) of Figure 29 have built-up edge as their main wear mechanisms, leading to delamination and tool failure. It is possible to observe intense delamination and chipping in tool (c) due to high BUE formation. Meanwhile, a much less intense and more stable BUE is also present in tool (d) throughout all cutting tests.

Due to its ductile nature, the machining of Super Duplex Stainless Steel causes a large amount of material to adhere to the cutting tool, generating BUE as well as

consequent delamination and chipping [20]. The built-up edge, consisting of workpiece particles that are adhered to the cutting tool, forms up and breaks away multiple times during the machining process. As the built-ups detach, they could carry away a part of the adhered cutting tool, which causes chipping. This will eventually lead to catastrophic tool failure.

BUE formation was the dominant failure mechanism in all of the tools with the exception of the AlTiN + TiB_2 bi-layer coated tool, in which the BUE was largely prevented. The resistance of the AlTiN + TiB_2 bi-layer coating to BUE formation can be attributed to its ability to self-adapt during machining. This adaptation involves the formation of thin tribofilms that improve the tribological conditions within the cutting zone.

Paiva et al. (2017) conducted similar experiments using duplex stainless-steel material (2507) with an AlTiN based PVD coated tool. This coating has been reported to generate a thin alumina film (Al_2O_3) known for its ceramic structure which enhances the wear performance of the cutting tool [36]. This thin alumina film has thermal barrier properties that mitigate the wear mechanisms in the cutting tool such as diffusion and oxidation.

Application of an AlTiN + TiB_2 bi-layer coating can prolong tool life, through the generation of Boron Oxide (B_2O_3) tribo-films. Hu et al. (2007) reported that Boron Oxide provides lubricious properties at elevated temperatures, which reduces the intensity of built-up edge formation.

Although the AlTiN + WC/C bi-layer coating is known to possess lubricious properties, its performance is inferior to that of AlTiN + TiB_2. Mo et al (2011) has conducted experiments with a lubricious WC/C coating under tribological conditions and found that under elevated loads and speeds, its coefficient of friction increases. [48] Also, the combination of poor surface roughness and low toughness contributes to its poor performance.

4.2.2 – Experiment B – $V_c = 130m/min$

Although a higher cutting speed is desirable for increasing the material removal rate, it can also lead to unexpected results.

A study of the wear performance of AlTiN, AlTiN + TiB_2, AlTiN + CrN and AlTiN + AlCrN bi-layer coated tools, was performed under finish turning operations listed in section 3. Life curves of the selected tools are described in figure 30.

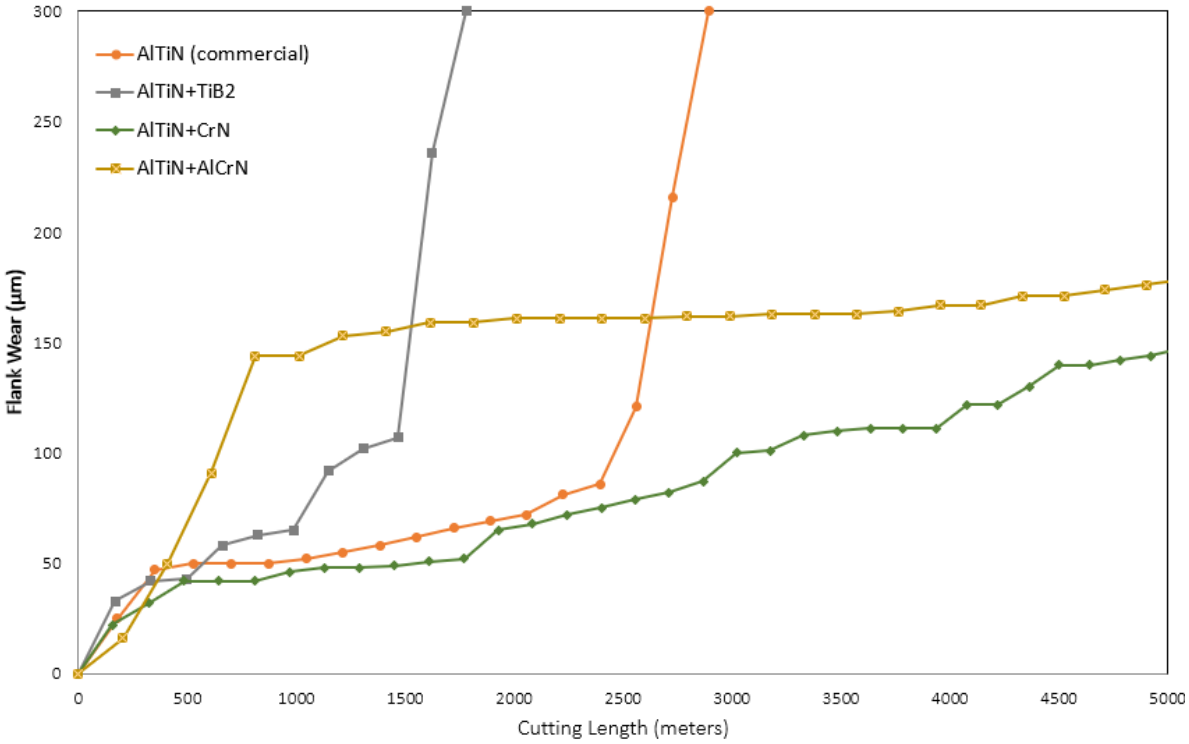

Figure 30. Flank wear versus cutting length (meters).

The AlTiN + CrN bi-layer has the best performance out of all of the tools tested in this experiment. The AlTiN + AlCrN bi-layer had also exhibited good tool life performance, not reaching the failure criteria until the end of the test. These bi-layer coatings undergo less damage than AlTiN + TiB_2 and monolayer AlTiN.

The cutting forces of each coating were recorded at cutting lengths of 300, 1000 and 3000m (or last pass before failure). The results are shown in figure 31.

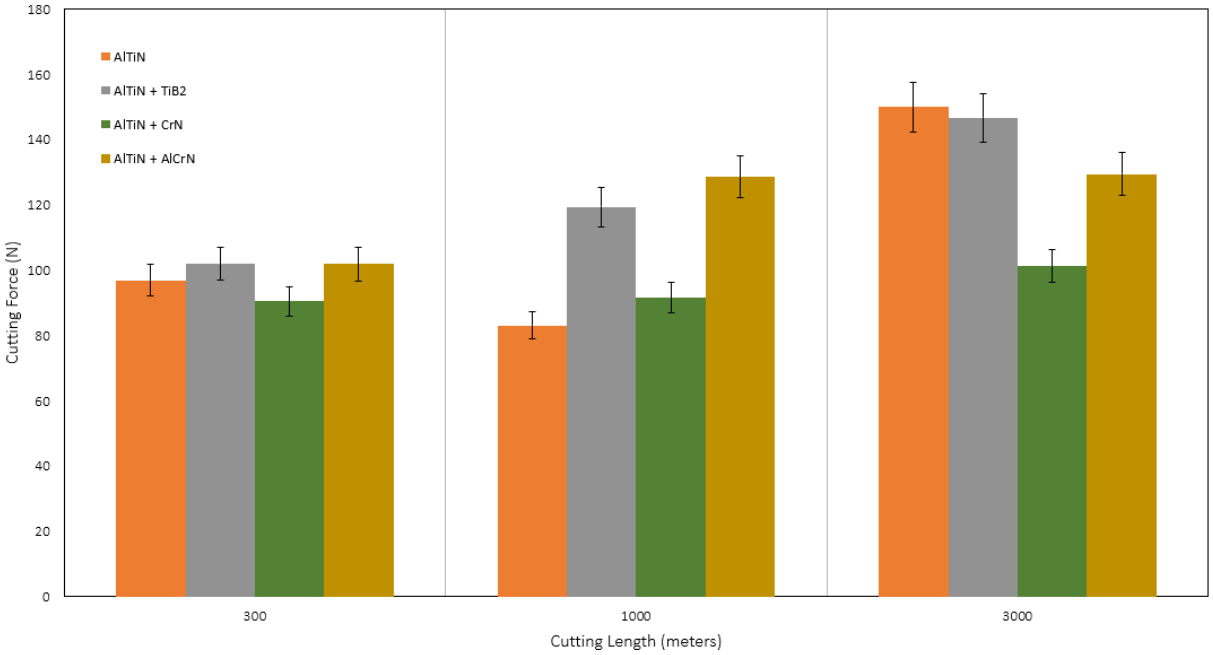

Figure 31. Cutting Forces data

In the beginning, all of the coated tools exhibited similar performance. However, at 3000 meters, the AlTiN coating and the AlTiN + TiB_2 bi-layer experienced a significant increase in their cutting forces. In comparison, AlTiN + CrN and AlTiN + AlCrN exhibited stable cutting forces during the machining operation.

Scanning electron microscopy images in figure 32 characterize the wear mechanisms of tool failure.

.

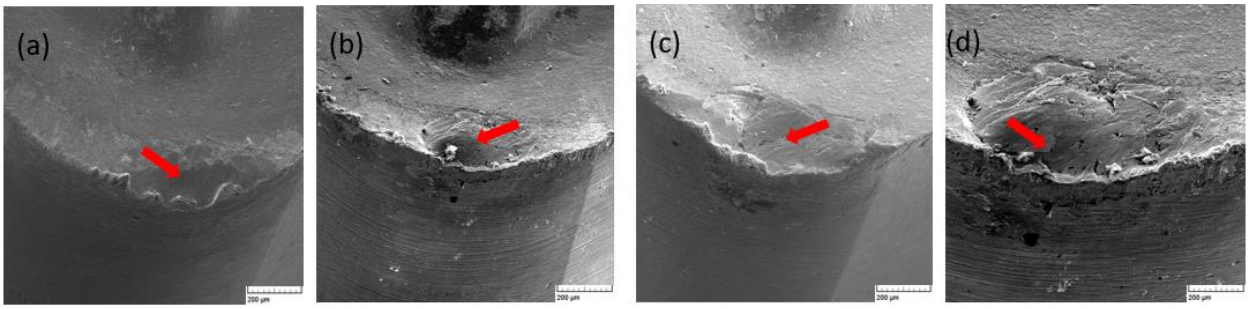

Figure 32. Worn turning tools SEM analysis: (a) AlTiN, (b) AlTiN + CrN, (c) AlTiN + AlCrN and (d) AlTiN + TiB_2.

As can be seen in figure 32, all coated tools except tool (b), coated with AlTiN + CrN, experience intensive crater wear. In tool (b) crater wear is also present but to a much lesser degree and greater stability.

Due to poor thermal conductivity and ductile behaviour, Super Duplex Stainless Steel will likely produce a high amount of crater wear on the cutting tool, which will result in rapid tool failure. Crater wear ensues when a very high temperature in combination with adhesive and diffusion wear are present at the tool-chip interface. [49] Lotfi (2010) has conducted a study of TiB_2 coating oxidation and reported that under very high temperatures, the Boron Oxide (B_2O_3) tribo-film delaminates from the coating. [50]

Chowdhury et al (2020) has conducted similar experiments on a TiAl6V4 aerospace alloy machined by an AlTiN PVD coated tool and a CrN PVD coated tool. The performance of the CrN coating was found to be superior to that of the AlTiN coating due to the formation of a thin film of chromium oxide (Cr_2O_3). This coating also

demonstrated a reduced coefficient of friction during machining, as well as lubricious/thermal barrier properties capable of reducing the intensity of crater wear.

AlTiN + CrN and AlTiN + AlCrN coatings have been shown to prolong tool life. Zhao et al. (2007) has found that at high temperatures, Chromium Oxide tribo-films possess lubricious and thermal barrier properties. [51]

The AlTiN + CrN coating also exhibited the lowest cutting force among the other tested tools. Once again, the thermal barrier and lubricious (Cr_2O_3) tribofilms [34] inhibit BUE formation as well as crater wear.

4.3 Chip Morphology Analysis

Chips were collected at the first pass of all the tools. Scanning electron microscopy images of either side of the surface as well as microhardness and microstructure analysis were acquired according to the experimental procedure outlined in section 3. The chip generated during machining had a sawtooth shape, which is typical for stainless steels.

4.3.1 – Experiment A – $V_c = 110 m/min$

SEM images of both surfaces of each coated tool, were taken during finish turning operations listed in section 3. These are shown in figure 33 at a cutting speed of 110m/min.

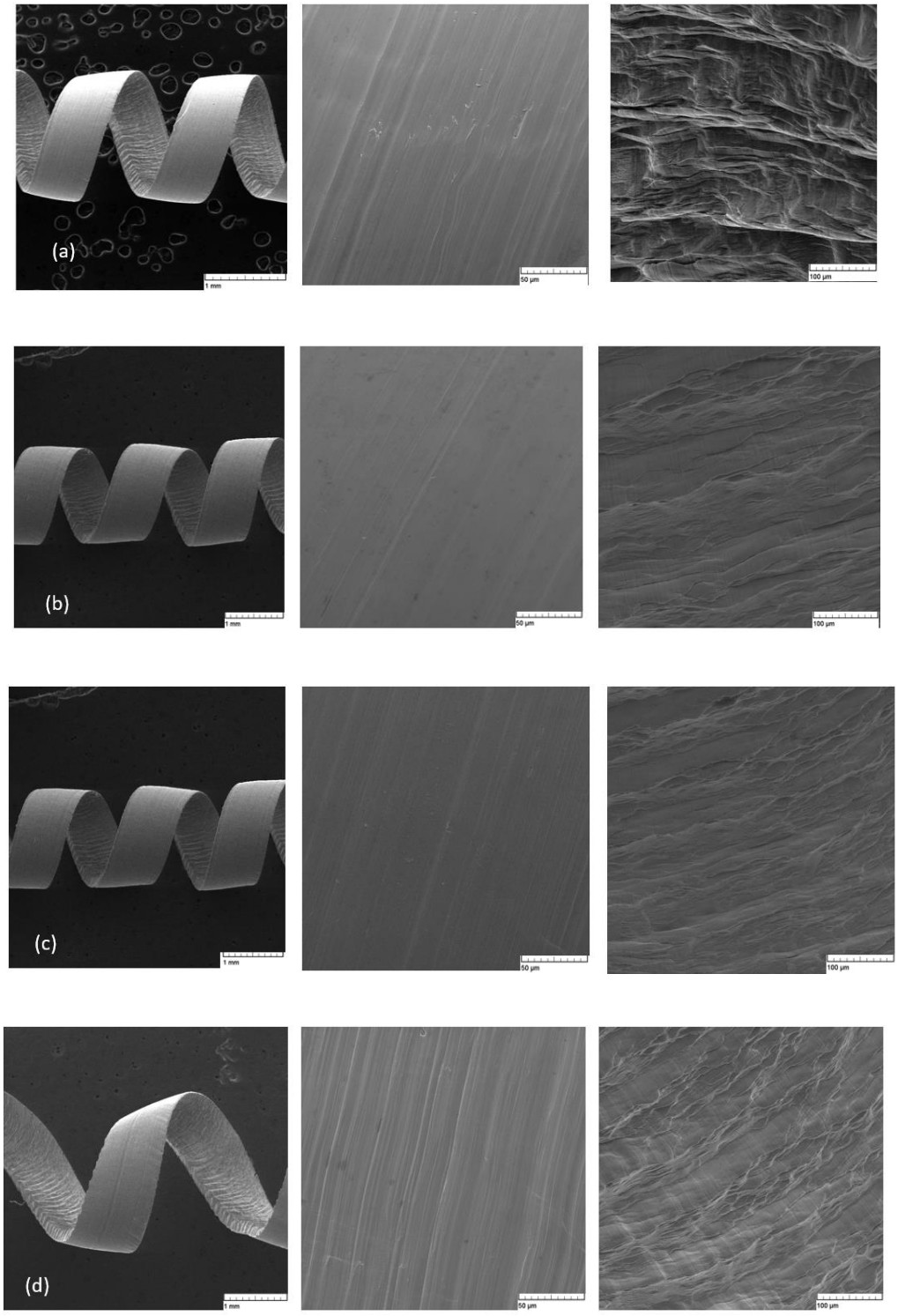

Figure 33. Chip as well as the top and bottom surfaces of each tool: (a) AlTiN, (b) AlTiN + TiB_2, (c) Uncoated and (d) AlTiN + WC/C

AlTiN + WC/C generates a more deformed chip with more plastically deformed shear bands. This deformed chip is likely to generate a higher cutting force due to the plastic deformation of the workpiece material, which will increase the cutting tool wear. Additionally, based on the conditions of experiment A, other coating combinations likely undergo similar chip formation.

The results of chip microhardness tests are depicted in figure 34.

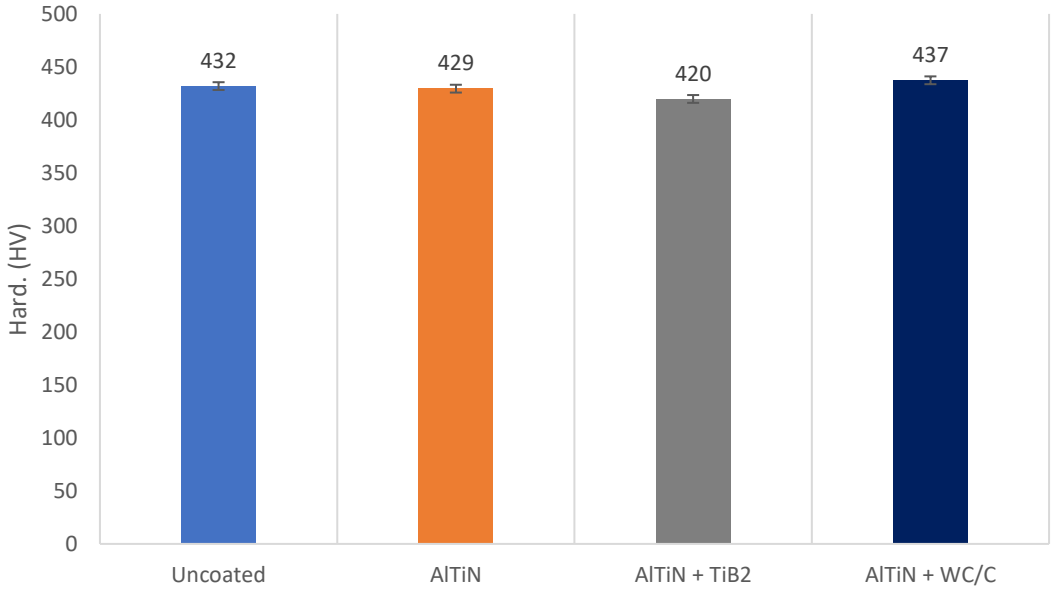

Figure 34. Microhardness of chips

As can be concluded from Figure 34, the chips' microhardness is related to cutting forces. When there is greater plastic deformation of the workpiece material, higher cutting forces are needed to remove it and at the same time, increase the microhardness of the chips. In this case, the cutting operation of AlTiN + TiB_2 is smoother compared to others,

possibly indicating that the chip slides more easily within the sticking-sliding region. This could ultimately reduce the cutting forces as well as the microhardness of removed workpiece material and therefore lead to an extension of tool life.

4.3.2 – Experiment B – $V_c = 130m/min$

SEM images of the chip, top and bottom surfaces of the three coated tools are depicted in Figure 35 under finish turning operations listed in section 3, at a cutting speed of 130m/min.

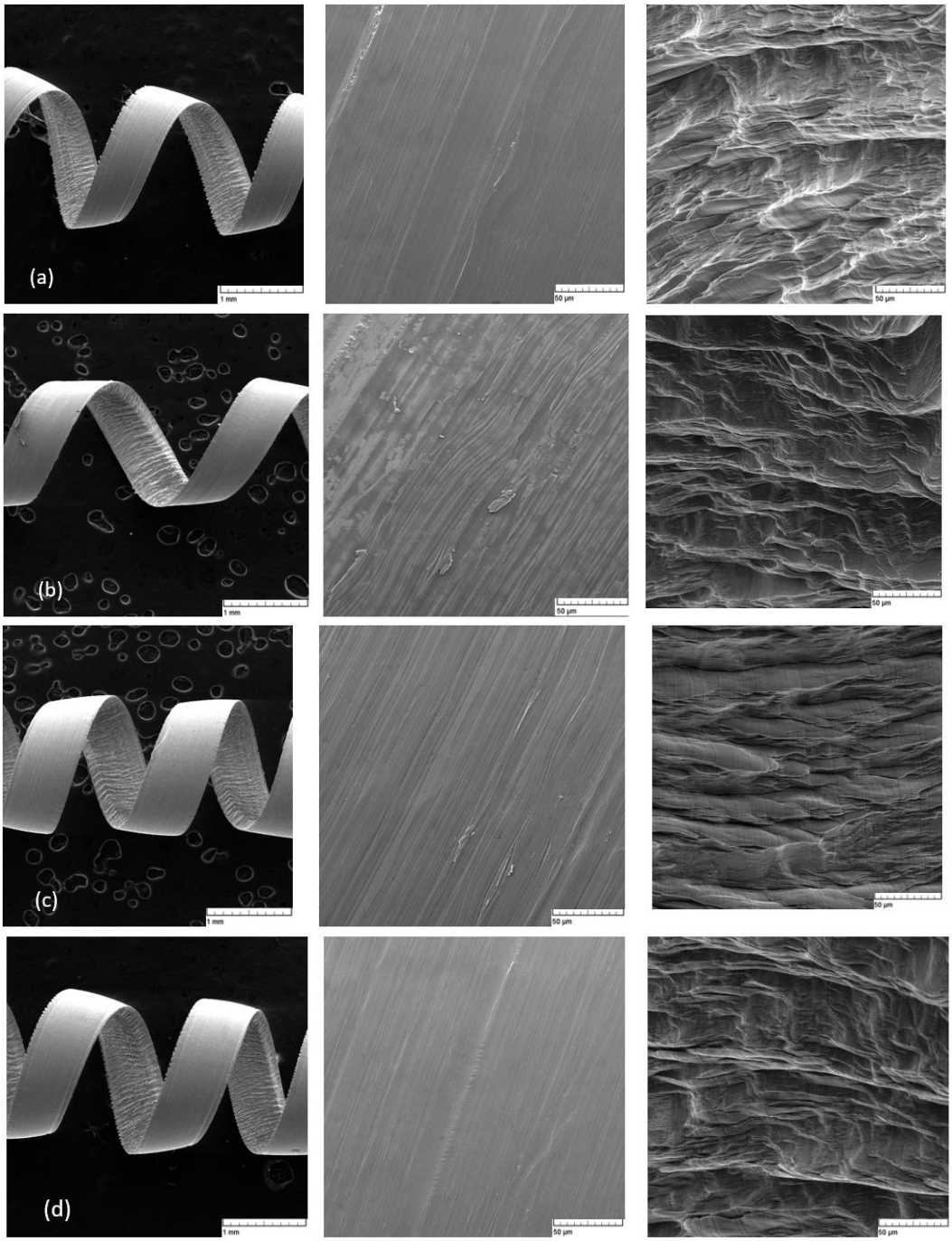

Figure 35. Chip, up and down surface: (a) AlTiN, (b) AlTiN + TiB_2, (c) AlTiN + CrN and (d) AlTiN + AlCrN

Figure 35 shows that a smoother chip with less plastically deformed shear bands is generated by the coated tools containing CrN. Other combinations, such as bi-layer AlTiN + TiB_2 and monolayer AlTiN feature more plastically deformed shear bands as well as a greater amount of removed deformed workpiece material. Having a higher plastic deformation, the interaction between the tool and the chip is more likely to generate higher cutting temperatures, leading to crater wear and tool failure.

Moreover, in addition to SEM images, the chip microhardness was also collected. The results can be seen in figure 36.

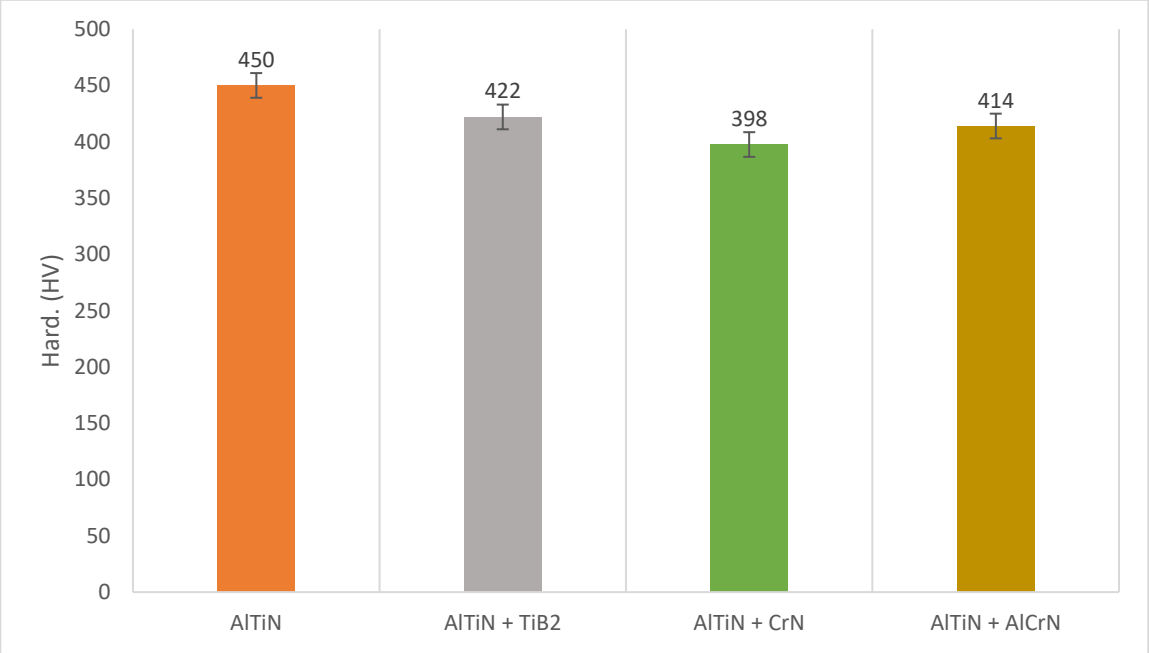

Figure 36. Microhardness of chips.

Fox-Rabinovich et al. (2016) performed a similar experiment on SDSS using different coatings at a cutting speed of 110m/min and 130m/min under a finish machining operation. He reported that the hardness distribution of removed workpiece material

(chips) can be altered by the sticking-sliding behaviour during tool-chip contact. At lower cutting speeds, the chips tend to harden at the tool-chip interface, whereas at higher cutting speeds, they can cause phase-transformation [strain-induced martensite] of the workpiece material into [33].

The CrN containing coatings exhibit superior results compared to the other coatings, which indicates that AlTiN and AlTiN + TiB_2 chip formation involves a phase transformation caused by the intense plastic deformation of the removed workpiece material.

The etched chip samples used in both experiments (AlTiN and AlTiN + TiB_2) are depicted in figure 37.

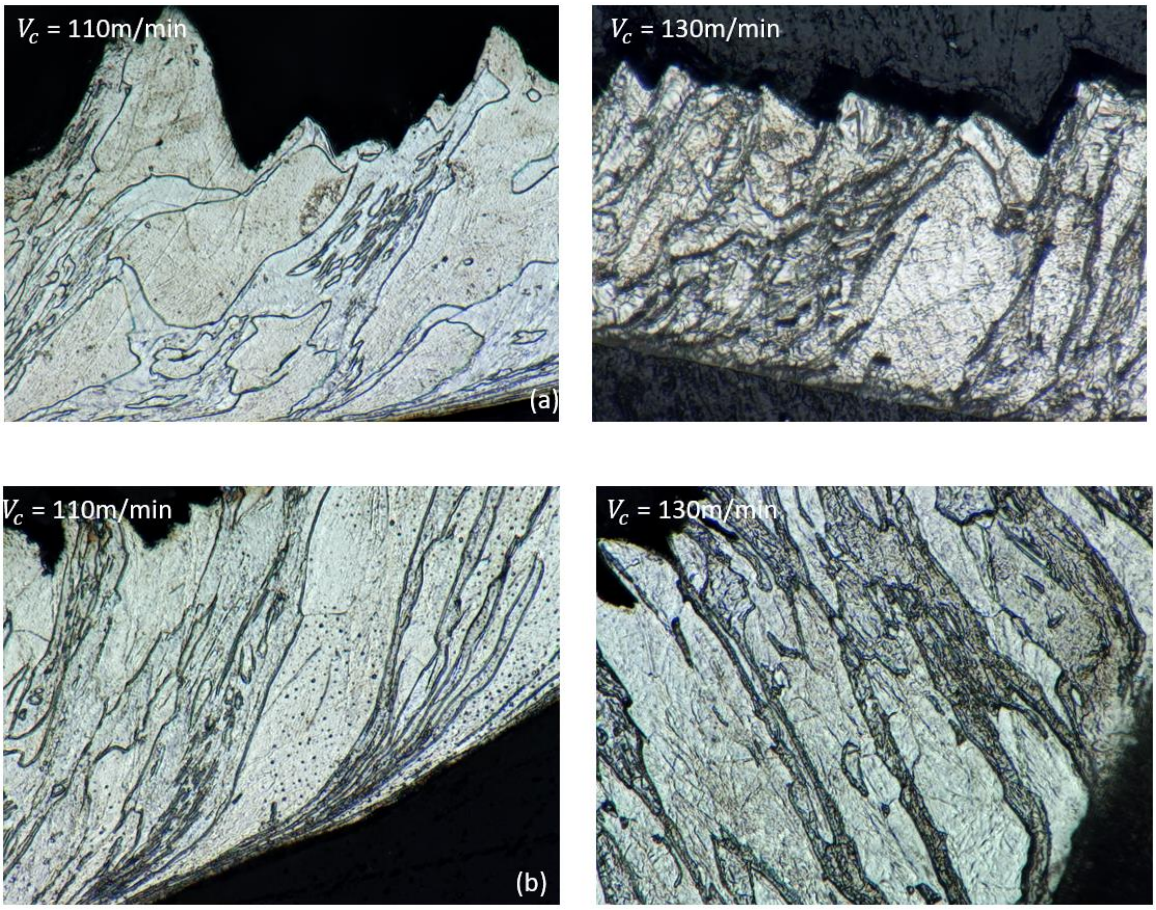

Figure 37. Etched chip samples (a) AlTiN and (b) AlTiN + TiB_2.

It is possible to observe in the acquired image of etched samples at both cutting speeds that the removed workpiece material underwent quite significant deformation at the higher cutting speed.

CHAPTER 5 – CONCLUSIONS

Coating characterization, wear performance and chip analysis of different HiPIMS PVD coatings applied on cutting tools during the finish turning of Super Duplex Stainless Steel, yielded the following conclusions:

- Coating Characteristics: The benchmark monolayer AlTiN coating featured the best results in terms of surface roughness, H/E ratio, adhesion to the substrate, and toughness.

  Although bi-layer HiPIMS coatings may potentially alter the properties of the monolayer, the AlTiN + TiB_2 coating had similar surface roughness, adhesion and residual stresses as the monolayer AlTiN coating, whereas the AlTiN +CrN bi-layer coating had very close adhesion and toughness but superior residual stresses. The bi-layer AlTiN + WC/C coating had the worst surface roughness and toughness.

- Tool Performance: During machining experiment A at lower cutting speeds ($V_c = 110 m/min$), the bi-layer HiPIMS AlTiN + TiB_2PVD coating exhibited the best results among the tools during machining, such as strongly reduced built-up edge formation and negligible surface damage. An SEM image revealed adhesion of workpiece material to the tool surface as the main wear mechanism, which

has led to built-up edge formation and eventual chipping. Additional cutting force data helps understand the the cutting behavior of coated tools. The solid performance of the AlTiN + TiB_2 bi-layer coating can be attributed to the formation of Boron Oxide (B_2O_3) lubricious tribo-films. This has reduced both cutting forces as well as adhesive interaction at the tool/chip interface.

Although the WC/C coating is known in literature to be a lubricious coating which reduces the coefficient of friction, its performance turned out to be quite poor at elevated temperatures observed in the experiments. [52] This can be attributed to its rough surface and low toughness, which lead to the intensive adhesion of workpiece material to the cutting tool and consequent rapid tool failure.

Monolayer AlTiN coatings can also generate thin alumina tribo-films with thermal barrier properties. At higher temperatures (above 600 $^{\circ}C$) the coefficient of friction of aluminum oxide (Al_2O_3), does not go down, which can result in rapid tool failure. In fact, the AlTiN coating exhibits the worst performance compared to the uncoated tool, most likely due to its detachment during the machining process.

In experiment B ($V_c = 130m/min$), the CrN/AlTiN bi-layer coating had the best performance out of all tested tools. The good performance this bi-layer coating can be attributed to the formation of a Chromium Oxide tribo-film which is known for its lubricious properties at high

temperatures. In this case, the tribo films were observed to form at around 750 $^{\circ}C$, reducing the temperatures and intensity of friction, and thereby ultimately prolonging the tool life. [51]

Although AlTiN + TiB_2 performed outstandingly in experiment A, its performance was quite poor during experiment B. The wear mechanism (characterized by SEM) of this coating was a combination of workpiece material adhesion and diffusion leading to crater wear formation and rapid tool failure. As cutting temperatures have risen along with cutting speed, Boron Oxide became delaminated from the surface of the tool (starting at 800 $^{\circ}C$). [50]

- Chip Analysis: During experiment A, the AlTiN + TiB_2 bi-layer coating produced less plastically deformed chips. This characteristic can be observed on the images of generated shear bands. The results and micro-hardness measurements demonstrate the same behaviour. During experiment B, the tool with AlTiN + CrN bi-layer coatings produced less plastically deformed chips, as can be seen in the images of the generated shear band and confirmed by micro-hardness measurements.

CHAPTER 6 – SUGGESTIONS FOR FUTURE WORK

Based on this study's conclusions, the following are suggested topics for future investigation:

- Evaluation of cutting temperature and its distribution throughout the cutting zone for the studied coatings during machining.
- Evaluation of the surface roughness of the machined part under lower and higher cutting speeds.
- Evaluation of tool life and wear mechanisms of the cutting tools with AlTiN/CrN bi-layer coatings under lower cutting speeds of 110 m/min.
- Evaluation of coating characteristics, tool life and wear mechanisms of the monolayer HiPIMS TiB_2, CrN and AlCrN coating under both studied cutting conditions.
- Evaluation of tool performance and wear phenomena under different cutting parameters such as higher feed rate, depth of cut and cutting speed.

References:

[1] World Oil Demand. (2020). Oil Energy Trends: Annual Statistical Review, 41(1), 53-61. doi:10.1111/oets.12068

[2] White, S. (2020, March 23). North America Stainless Steel Round Bar Market Is Forecast to Reach Beyond $2.1 Billion by 2022. Retrieved November 30, 2020, from https://sarawhite593.medium.com/north-america-stainless-steel-round-bar-market-is-forecast-to-reach-beyond-2-1-billion-by-2022-8216abda9aee

[3] Diniz, A. E., Machado, Á R., Corrêa, J. G. (2016). Tool wear mechanisms in the machining of steels and stainless steels. The International Journal of Advanced Manufacturing Technology, 87(9-12), 3157-3168. doi:10.1007/s00170-016-8704-3

[4] Junior, C. A., Diniz, A. E., Bertazzoli, R. (2013). Correlating tool wear, surface roughness and corrosion resistance in the turning process of super duplex stainless steel. Journal of the Brazilian Society of Mechanical Sciences and Engineering, 36(4), 775-785. doi:10.1007/s40430-013-0119-6

[5] Mangili, P. V., Ahón, V. R. (2019). Comparison of Pvt Correlations for Predicting Crude Oil Properties: The Brazilian Campos Basin Case Study. Brazilian Journal of Petroleum and Gas, 13(3), 129-157. doi:10.5419/bjpg2019-0013

[6] Practical guidelines for the fabrication of duplex stainless steel. 2nd ed. 2009, International Molybdenum Association.

[7] Tahchieva, A., Llorca-Isern, N., Cabrera, J. (2019). Duplex and Superduplex Stainless Steels: Microstructure and Property Evolution by Surface Modification Processes. Metals, 9(3), 347. doi:10.3390/met9030347

[8] Ahmed, Y. S., Paiva, J. M., Bose, B., Veldhuis, S. C. (2019). New observations on built-up edge structures for improving machining performance during the cutting of superduplex stainless steel. Tribology International, 137, 212-227. doi:10.1016/j.triboint.2019.04.039

[9] Kim, S., Kang, K., Kim, M., Lee, J. (2015). Low-Temperature Mechanical Behavior of Super Duplex Stainless Steel with Sigma Precipitation. Metals, 5(3), 1732-1745. doi:10.3390/met5031732

[10] Fortan, M., Dejans, A., Debruyne, D., Rossi, B. (2017). The strength of stainless steel fillet welds using GMAW, Proceedings of Stainless Steel in Structures: Fifth International Experts Seminar, Vol.13.

[11] Pohl, M., Storz, O., Glogowski, T. Effect of intermetallic precipitations on the properties of duplex stainless steel, Mater. Charact., vol. 58, no. 1, pp. 65–71, Jan. 2007.

[12] Lippold, J. C., & Kotecki, D. J. (2005). Welding metallurgy and weldability of stainless steels. Hoboken, NJ: John Wiley.

[13] Bhadeshia, H.K.D.H., Honeycomb, R., Steels: Microstructure and Properties, 3rd edition Oxford - UK: Elsevier, 2006.

[14] Nilsson, J.-O. (1992) Super duplex stainless steels, Materials Science and Technology, 8:8, 685-700, DOI: 10.1179/mst.1992.8.8.685

[15] Akisanya, A. R., Obi, U., Renton, N. C. (2012). Effect of ageing on phase evolution and mechanical properties of a high tungsten super-duplex stainless steel. Materials Science and Engineering: A, 535, 281-289. doi:10.1016/j.msea.2011.12.087

[16] Davis, J.R., Stainless Steel - ASM Speciality Handbook, 2nd ed. USA: ASM International, 2000.

[17] Tavares, S.S.M., Pardal, J.M., Lima, L.D., Bastos, I.N., Nascimento, A.M., de Souza, J.A., Characterization of microstructure, chemical composition, corrosion resistance and toughness of a multi pass weld joint of superduplex stainless steel UNS S32750, Mater. Charact., vol. 58, no. 7, pp. 610–616, Jul. 2007.

[18] Gunn, R.N., Duplex stainless steels, 1st edition. Woodhead Publishing Limited, 1997.

[19] Stephenson, D. A. (2019). Metal Cutting Theory and Practice. CRC Press.

[20] Shaw, M.C. Metal Cutting Principles, Second Edi. 2004.

[21] Trent, E. M., Wright, P. K., Metal Cutting, 4th Edition. Butterworth Heinemann, 2000.

[22] Monroy Vazquez K.P., Giardini C., Ceretti E. (2014) Cutting Force Modeling. In: The International Academy for Production Engineering, Laperrière L., Reinhart G.

(eds) CIRP Encyclopedia of Production Engineering. Springer, Berlin, Heidelberg. https://doi.org/10.1007/978-3-642-20617-7_6399

[23] Gekonde, H.O., Subramanian, S. (2002). Tribology of tool–chip interface and tool wear mechanisms. Surface and Coatings Technology, 149(2-3), 151-160. doi:10.1016/s0257-8972(01)01488-8

[24] Avevor, Y., Moufki, A., Nouari, M. (2017). Analysis of the Frictional Heat Partition in Sticking-sliding Contact for Dry Machining: An Analytical-Numerical Modelling. Procedia CIRP, 58, 539-542. doi:10.1016/j.procir.2017.03.334

[25] Montay, G., Cherouat, A., Nussair, A. Lu, J. (2004). Residual stresses in coating technology. Journal of Materials Science and Technology. 20. 81-84.

[26] Johnson, C., Ruud, J., Bruce, R., Wortman, D. (1998). Relationships between residual stress, microstructure and mechanical properties of electron beam–physical vapor deposition thermal barrier coatings. Surface and Coatings Technology, 108-109, 80-85. doi:10.1016/s0257-8972(98)00668-9

[27] Outeiro, J. (2018) Residual Stresses in Machining Operations. In: The International Academy for Production, Laperrière L., Reinhart G. (eds) CIRP Encyclopedia of Production Engineering. Springer, Berlin, Heidelberg. https://doi.org/10.1007/978-3-642-35950-7_16811-1

[28] Alhadeff, L., Marshall, M., Slatter, T., (2019). The influence of tool coating on the length of the normal operating region (steady-state wear) for micro end mills. Precision Engineering, 60, 306-319. doi:10.1016/j.precisioneng.2019.07.018

[29] ISO 3685: Tool-life testing with single-point turning tools. (1993). Ginebra: ISO.

[30] Matthews A., Holmberg K. (2013) PVD and CVD Coatings. In: Wang Q.J., Chung YW. (eds) Encyclopedia of Tribology. Springer, Boston, MA. https://doi.org/10.1007/978-0-387-92897-5_724

[31] Aliofkhazraei, M., Ali, N. (2014). PVD Technology in Fabrication of Micro- and Nanostructured Coatings. Comprehensive Materials Processing, 49-84. doi:10.1016/b978-0-08-096532-1.00705-6

[32] Fox-Rabinovich, G. S., Totten, G. E. (2007). Self-organization during friction: Advanced surface-engineered materials and systems design. Boca Raton: CRC Press - Taylor Francis.

[33] Fox-Rabinovich, G., Paiva, J., Gershman, I., Aramesh, M., Cavelli, D., Yamamoto, K., Veldhuis, S. (2016). Control of Self-Organized Criticality through Adaptive Behavior of Nano-Structured Thin Film Coatings. Entropy, 18(8), 290. doi:10.3390/e18080290

[34] Paiva, J. M., Shalaby, M. A., Chowdhury, M., Shuster, L., Chertovskikh, S., Covelli, D., Veldhuis, S. C. (2017). Tribological and Wear Performance of Carbide Tools with

TiB2 PVD Coating under Varying Machining Conditions of TiAl6V4 Aerospace Alloy. Coatings, 7(11), 187. doi:10.3390/coatings7110187

[35] Chowdhury, M., Bose, B., Yamamoto, K., Shuster, L., Paiva, J., Fox-Rabinovich, G., Veldhuis, S. (2020). Wear performance investigation of PVD coated and uncoated carbide tools during high-speed machining of TiAl6V4 aerospace alloy. Wear, 446-447, 203168. doi:10.1016/j.wear.2019.203168

[36] Fox-Rabinovich, G. S., Gershman, I. S., Yamamoto, K., Aguirre, M. H., Covelli, D., Arif, T., Veldhuis, S. (2016). Surface/interface phenomena in nano-multilayer coating under severing tribological conditions. Surface and Interface Analysis, 49(7), 584-593. doi:10.1002/sia.6196

[37] Alami, J., Persson, P. O., Music, D., Gudmundsson, J. T., Bohlmark, J., Helmersson, U. (2005). Ion-assisted physical vapor deposition for enhanced film properties on nonflat surfaces. Journal of Vacuum Science Technology A: Vacuum, Surfaces, and Films, 23(2), 278-280. doi:10.1116/1.1861049

[38] Tiron, V., Ursu, E., Cristea, D., Munteanu, D., Bulai, G., Ceban, A., Velicu, I. (2019). Overcoming the insulating materials limitation in HiPIMS: Ion-assisted deposition of DLC coatings using bipolar HiPIMS. Applied Surface Science, 494, 871-879. doi:10.1016/j.apsusc.2019.07.239

[39] Paiva, J. M., Torres, R. D., Amorim, F. L., Covelli, D., Tauhiduzzaman, M., Veldhuis, S., Fox-Rabinovich, G. (2017). Frictional and wear performance of hard

coatings during machining of superduplex stainless steel. The International Journal of Advanced Manufacturing Technology, 92(1-4), 423-432. doi:10.1007/s00170-017-0141-4

[40] Chinchanikar, S., Choudhury, S. (2014). Hard turning using HiPIMS-coated carbide tools: Wear behavior under dry and minimum quantity lubrication (MQL). Measurement, 55, 536-548. doi:10.1016/j.measurement.2014.06.002

[41] Li, G., Sun, J., Xu, Y., Xu, Y., Gu, J., Wang, L., Li, L. (2018). Microstructure, mechanical properties, and cutting performance of TiAlSiN multilayer coatings prepared by HiPIMS. Surface and Coatings Technology, 353, 274-281. doi:10.1016/j.surfcoat.2018.06.017

[42] Tiron, V., Ursu, E., Cristea, D., Munteanu, D., Bulai, G., Ceban, A., Velicu, I. (2019). Overcoming the insulating materials limitation in HiPIMS: Ion-assisted deposition of DLC coatings using bipolar HiPIMS. Applied Surface Science, 494, 871-879. doi:10.1016/j.apsusc.2019.07.239

[43] Ebnesajjad, S., Ebnesajjad, C. (2013). Surface Treatment of Materials for Adhesive Bonding, second ed., Elsevier, 2013.

[44] Matei, A.A., Pencea, I., Stanciu, S.G., Hristu, R., Antoniac, I., Ciovica, E., Sfat, C.E., Stanciu, G.A. (2015). Structural characterization and adhesion appraisal of TiN and TiCN coatings deposited by CAE-PVD technique on a new carbide composite cutting

tool, J. Adhes. Sci. Technol. 29 2576–2589, https://doi.org/10.1080/01694243.2015.1075857.

[45] Chowdhury, M., Bose, B., Yamamoto, K., Shuster, L., Paiva, J., Fox-Rabinovich, G., Veldhuis, S. (2020). Wear performance investigation of PVD coated and uncoated carbide tools during high-speed machining of TiAl6V4 aerospace alloy. Wear, 446-447, 203168. doi:10.1016/j.wear.2019.203168

[46] Mo, J., Zhu, M., Leyland, A., Matthews, A. (2013). Impact wear and abrasion resistance of CrN, AlCrN and AlTiN PVD coatings. Surface and Coatings Technology, 215, 170-177. doi:10.1016/j.surfcoat.2012.08.077.

[47] Zhang, X., Beake, B.D., Zhang, S., Chapter 2-Toughness evaluation of thin hard coatings and films, in: Thin Films and Coatings: Toughening and Toughness Characterization, CRC Press, Taylor and Francis Group, Boca Raton, NW, USA, 2015.

[48] Mo, J., Zhu, M. (2011). Tribological investigation of WC/C coating under dry sliding conditions. Wear, 271(9-10), 1998-2005. doi:10.1016/j.wear.2010.12.016.

[49] Rubenstein C. (1976). An Analysis of Crater Wear Based on the Adhesive Wear Mechanism. In: Koenigsberger F., Tobias S.A. (eds) Proceedings of the Sixteenth International Machine Tool Design and Research Conference. Palgrave, London. https://doi.org/10.1007/978-1-349-81544-9_75.

[50] Lotfi, B. (2010). Elevated temperature oxidation behavior of HVOF sprayed TiB2 cermet coating. Transactions of Nonferrous Metals Society of China, 20(2), 243-247. doi:10.1016/s1003-6326(09)60129-1.

[51] Zhao, C., Nie, X., Tjong, J. (2018). Renewable Cr2O3Nanolayer on Cr(W)N Surface for Seizure Prevention at Elevated Temperatures. ACS Applied Materials Interfaces, 10(30), 25787-25793. doi:10.1021/acsami.8b07938.

[52] Lofaj, F., Mikula, M., Grančič, B., Cempura, G., Hornak, P., Kus, P., Kottfer, D. (2011). Tribological properties of TiB x and WC/C coatings. Ceramics Silikáty. 55. 305-311.